Neutron Powder Diffraction – New Opportunities in Hydrogen Location in Molecular and Materials Structure

Chick C. Wilson*[,1], Paul F. Henry[2, 3], Marc Schmidtmann[4], Valeska P. Ting[5] , Edward Williams[1] and Mark T. Weller[1]

1 – Department of Chemistry, University of Bath, Bath BA2 7AY, UK
2 – European Spallation Source ESS AB, PO Box 176, S-221 00 Lund, Sweden
3 – Department of Chemical and Biological Engineering, Chalmers University of Technology, SE412-96 Gothenburg, Sweden
4 – Department of Chemistry, Carl von Ossietzky University of Oldenburg, Carl-von-Ossietzky-Str. 9-11, 26129 Oldenburg, Germany
5 – Department of Chemical Engineering, University of Bath, Bath BA2 7AY, UK

* Contact author: C.C.Wilson@bath.ac.uk

Abstract

The potential of neutron powder diffraction in the location of hydrogen atoms in molecular materials and inorganic-molecular complexes is reviewed. Advances in instrumentation and data collection techniques that have made this field accessible are reviewed, along with a wide range of applications carried out by our collaboration investigating functional materials, hydrogen-containing minerals and molecular compounds. Some of the limitations in this area, particularly for molecular systems, are also addressed.

1. Introduction

Hydrogen is a key element whose functionality in inorganic material systems stretches from geochemical materials (e.g. clay minerals, cements), through key inorganic compounds (e.g. catalysts, co-ordination complexes and hydroxides/hydrates) and materials (e.g. polymers, hydrogen storage media, proton conductors/fuel cell components) to supramolecular and framework systems (e.g aluminosilicates, solvates and clathrates). The role of hydrogen in the structures (and hence derived applications) of these materials is thus of the utmost importance but one that, until recently, experimental methods generally failed to address, or could only do so in selected cases at great expense and considerable effort. Determination of the position of hydrogen in a material, whether it be a naturally occurring hydrate/hydroxide, a cement, a hydride/hydrogen storage material, a solvate or an organometallic compound has traditionally been difficult, time-consuming, expensive and imprecise, even where possible. However, knowledge of the distribution of hydrogen is central to understanding behaviours such as polymorphism, hydrogen bonding and three-dimensional structure definition, proton diffusion

pathways and levels of uptake in hydrogen storage materials, physical properties ranging from ferro-electricity to the elastic properties of polymers, and reaction mechanisms. Therefore the implementation and application of methodology that allows *routine* hydrogen position definition from *readily available* material (i.e. small easily synthesised quantities and in polycrystalline/small single crystal (≤50μm) form) is both of widespread application and key importance.

In the work described here, development of the application of powder neutron diffraction methods in an optimised fashion to such materials is shown to have the capability to reveal structural information in a range of hydrogen-containing materials. A range of recent studies will be summarized, to illustrate the potential of this new capability. The powerful complementary use of both X-ray and computational methods with neutron powder diffraction in these studies will also be highlighted. The aim in this Review is not to provide a detailed account of the different materials studied, but to highlight the power of the methods of approach we have been systematically developing to access more accurate and different chemistry. It draws on a range of examples from our own collaborative work, which has recently focused on this theme [1].

In this review, we have deliberately focused the choice of examples on our own programme of work, as this has involved a wide-ranging and systematic investigation of a range of materials types, with a range of degrees of hydrogen content, and in parallel with this have undertaken detailed technical assessments of the performance of NPD in this work. By focusing on the possibilities in a selected range of materials in this way, we aim to highlight the capabilities opened up by recent technical advances, while also specifically highlighting areas where the information targeted from some of the materials studies has not been obtained. We wish to present these so-far unsuccessful studies to encourage further and future solutions in this area. Our focus on molecular materials as an important, developing, element of neutron powder studies of hydrogen-containing systems has resulted in the majority of these "unsuccessful" cases, which are reported here in this context. In order to focus on this systematic approach, and to establish the scope and some of the limitations of current NPD in this area, we have therefore sought to present a set of findings that cover a range of materials types, following a consistent methodology and largely based on measurements made on a single, well-optimised instrument. In this way we hope that this review will produce a coherent introduction to possibilities in this area, while naturally acknowledging that many others have carried out work in this field, with a range of successes in determining the structure of hydrogenous materials from neutron powder data. In many of these studies, the primary focus has not necessarily been on the determination of hydrogen parameters specifically, but on structures containing hydrogen, while the focus here is on hydrogen atom determination. However, amongst many examples

of previous work that offer an indication of the wide scope of this, are studies of potassium hydrogen selenates [2], pure organic molecules [3], hydrated salts [4], clathrates [5], organometallic complexes [6] including joint neutron powder / single crystal X-ray studies [7], *in situ* studies [8] and hydrides for energy applications [9].

2. Neutron diffraction

In contrast to other techniques such as X-ray or electron diffraction, neutrons are scattered by the nucleus, rather than the electrons in an atom. While the scattering power for those forms of radiation that scatter from the electrons strongly depends on the atomic number and, for example, the scattered intensity for X-ray diffraction is proportional to Z^2, for neutrons this interaction depends on the properties of the scattering nucleus. The consequence of this is that the scattering power, given by the scattering length, does not vary monotonically with Z.

This has several beneficial consequences for the application of neutron diffraction in the study of a wide range of materials:

- Elements with similar Z-values generally have substantially different scattering cross sections, offering a direct method of distinguishing neighbouring elements;
- Isotopes of the same element generally have substantially different scattering lengths for neutrons, making the technique of isotopic substitution very powerful;
- Of particular relevance here, it is possible with neutron diffraction to determine the parameters of light atoms, such as hydrogen, in the presence of heavier ones more accurately. For example, hydrogen atoms are determined around an order of magnitude more accurately with neutrons than X-rays in the presence of carbon atoms. Light atoms such as hydrogen and carbon can also be located with high levels of precision even in the presence of heavy metals;
- One significant experimental advantage of neutron diffraction is the flexibility in the available sample environment. As neutrons do not suffer absorption on passing through sample chamber walls, neutron diffraction can, for example, be carried out routinely at a wide range of temperatures, typically from below 4K to 1500K. The ability to collect data over such a temperature range is becoming more routinely available for X-ray experiments also, but is by no means universal.

There are disadvantages, however:

- The magnitudes of X-ray scattering factors are higher than those for neutrons and this, coupled with the relatively low flux of neutron sources, means that the size of samples required for neutron diffraction are generally larger than for X-rays. Traditionally, data collection times for neutron diffraction have also been longer than for X-ray diffraction;
- In addition to its favourable coherent scattering length – leading to a high visibility of hydrogen in neutron diffraction experiments – the common isotope ^{1}H has a very large incoherent scattering cross section (Figure 1), leading to a very high background contribution. This not an issue for neutron single crystal diffraction studies of small molecular or molecule-inorganic systems, but does cause significant issues for neutron powder diffraction, where the large incoherent scattering cross-section leads to high background, that are neutron energy and so wavelength dependent and which are difficult to model due to the sample dependence of the incoherent scattering;

Figure 1 – Comparison of ^{1}H (H) and ^{2}H (D) incoherent scattering cross-sections, showing the reduction in this cross section for D (represented by the light area).

- The neutron inelastic scattering cross sections of hydrogen-containing compounds, for neutrons with wavelengths frequently used in neutron diffraction, 1-2 Å, increase rapidly with temperature where there is significant hydrogen atom motion through vibrational or torsional modes. Therefore in systems containing molecular hydrogen species, such as organic compounds or hydrates, at high temperatures the elastic scattering (diffraction) becomes more difficult to discern and therefore measure accurately.

There are several potential routes to overcoming these difficulties, each of which raises its own issues:

- For neutron single crystal diffraction, grow large single crystals – experimentally this can often be difficult;
- For neutron powder diffraction, deuterate the material – again this can be difficult experimentally, with syntheses of molecular materials involving extensive chemistry that would also have to be carried out using deuterated starting materials. Perhaps more seriously, the chemical and physical properties of deuterated materials can in many cases be substantially different. Thus in many cases it is crucial that experiments are carried out on fully hydrogenous materials;

- For the reduction of data collection time in general, enhance the available useful flux on the sample. This can be achieved by increasing the flux available from sources – which can be difficult, expensive and achievable only on very long timescales – or by optimising instruments on existing sources to maximise counts rate (and in parallel to minimise background where possible). Both new sources and new instrumentation are being developed; recent results in high throughput neutron diffraction have benefited primarily from the new instrumentation that has been made available over the last decade, while new sources offer further huge future potential.

2.1 Hydrogen by Neutron Powder Diffraction

As noted above, due to the weak scattering of X-rays by hydrogen (relative to that of other elements), neutron diffraction is the obvious choice for locating hydrogen. However, the incoherent scattering of neutrons by the ^{1}H isotope leads to high backgrounds and noisy data sets using standard experimental set-ups and instrumentation, from which extraction of hydrogen positions is *normally* so poor as to be not worthwhile. Such problems have, in a very few cases, been overcome by sample deuteration or single crystal neutron studies but these techniques are of very limited applicability due to the cost and time for deuteration or the impossibility of growing the large single crystals that are necessary due to low neutron fluxes. Furthermore deuteration may be impossible to achieve, for example with mineral samples with non-mobile protons or may alter the property of interest such as ferroelectricity associated with H/D ordering.

Among the major drivers for establishing the routine use of neutron powder diffraction for hydrogen atom location is that the growth of large single crystals for neutron diffraction or the routine deuteration of materials to reduce the incoherent background are equally challenging experimentally, and in many cases prohibitively expensive or practically impossible. To achieve this, the problems with incoherent scattering from hydrogenous polycrystalline materials can be mitigated through the correctly engineered use of the new generation of very high flux powder diffractometers such as GEM at the ISIS spallation neutron source in the UK, D20 at the reactor source at ILL, Grenoble, POWGEN at the US Spallation Neutron Source and specialist optimised instruments such as PLANET at J-PARC. The new capabilities realized by these methods allow incoherent scattering to be rapidly averaged and thus easily subtracted from the raw data producing reasonably good quality diffraction data from small samples.

Furthermore by combining such data with that obtained from other methods (particularly single crystal X-ray diffraction, which can, of course, be obtained from relatively small single crystals) on the identical

material, the additional information inherent within powder neutron data can be extracted. It should be noted that while high resolution, high intensity (powder) diffractometers on synchrotron X-ray sources potentially offer the data (numbers of reflections + well determined intensities) required to extract hydrogen positions, routine determination of these positions is not generally possible due to the weak scattering from hydrogen and its extremely rapid angular loss due to the highly diffuse electron distribution and thermal motion. Appropriately optimised, powder neutron diffraction (either alone or when combined with easily accessed X-ray single crystal methods) can provide the method of choice for many problems in structure determination of hydrogen-containing materials.

2.2 Neutron crystallography of molecular materials

Neutron scattering has played a major role in developing an understanding of how structure affects the properties of crystalline materials, in areas of relevance to much of modern structural chemistry [10]. Areas in which neutron diffraction can play a key role include organic materials, pharmaceuticals, increasingly large biological macromolecules, zeolites, polymer electrolytes, battery materials, catalysts, superconductors, time-resolved and *in situ* studies, and chemical magnetism.

Considering molecular systems specifically, much of the focus in previous work has been on single crystal neutron diffraction [10, 11]. For example, hydrogen atoms (e.g. hydride ligands) can be located in organometallic complexes far more reliably than by any other method, while much of the structural work on hydrogen bonded systems (e.g. amino acids, nucleic acid components, carbohydrates, cyclodextrins) has used neutron diffraction. In addition, determination of the hydrogen anisotropic displacement parameters in short O…O hydrogen bonds allows, for example, the deduction of the shape of the potential well in which the atom sits [12]. Neutron single crystal diffraction has an important role in defining the patterns of “weak” intermolecular interactions in complex molecular and supramolecular structures, as these often crucially involve hydrogen atoms [13, 14]. This leads directly to a strong impact in the expanding area of molecular and crystal engineering.

Neutron diffraction also gives complementary information to X-ray diffraction for charge density studies [15, 16]. In X-N studies the neutron parameters fix the nuclear positions and the X-ray data determine the electron density involved in bonding and non-bonding interactions. Neutron diffraction experiments are often carried out under extreme conditions of sample environment such as high and low temperature, under controlled atmospheres, high pressure and in chemical reaction cells. More recently there has been

a focus on using single crystal neutron diffraction in the study of the evolution of molecular systems [11, and references therein] – a type of investigation more traditionally associated with powder diffraction techniques – yielding accurate atomic parameters whose trends as a function of external variable can give important information on structure-property relationships.

Recent variable temperature (and variable pressure) neutron diffraction studies of molecular structures containing hydrogen bonds have shown that the hydrogen atom of interest can exhibit interesting behaviour under varying conditions [17, 18, 19, 20, 21, 22, 23, 24, 25, 26], along with examples where variable temperature X-ray studies have provided valuable, complementary, information in which indications of H atom behaviour have been obtained, without necessarily accessing the required accuracy and precision of the relevant parameters [27, 28, 29, 30, 31, 32]. There has also been an increased emphasis on harnessing the information available from complementary diffraction and computational studies [33], 34, [35].

Studies such as this have dramatically enhanced the capabilities of single crystal neutron diffraction to access information on molecular materials, but the restrictions on neutron single crystal diffraction mentioned above limit the range of materials to which the technique can be applied. X-ray single crystal diffraction, on the other hand, offers access to a far wider range of systems, notably by allowing the study of samples with smaller crystals and in shorter data collection times, while leaving under-determined the often crucial hydrogen atoms parameters in many of these systems. Combining the use of single crystal XRD with powder neutron diffraction thus offers an alternative, combined radiation, approach to structure determination of hydrogenous systems.

There are obvious advantages in using a combination of complementary X-ray and neutron diffraction data for the study of hydrogenous materials. In an early example, a combination of single crystal X-ray and single crystal neutron diffraction data was used to investigate hydrogen positions in $[Co[NH_3]_6][CuCl_5]$, though simultaneous refinement of the structure using both data sets was not attempted [36], while more recently the input of heavy atom positions from SXD into SND data was used for the calculation of difference Fourier maps resulting in the discovery of five-coordinate hydrogen in the $[H_2Rh_{13}(CO)_{24}]^{3-}$ cluster complex [37]. Simultaneous refinement against XPD and NPD data has been successfully applied to the determination of hydrogen atom positions in the organic molecules chlorothiazide and hydrochlorothiazide [38], the simple hydrated salt $Cs_2C_2O_4.H_2O$ [39] and has recently been shown also to

be effective for complicated inorganic materials. Inability to grow a single crystal of $Li_4BH_4(NH_2)_3$ led to the use of combined X-ray and neutron powder diffraction data sets for crystal structure investigation [40]. Simultaneous refinement using synchrotron XPD and NPD data has also been used to deduce the structure of $Nb_2O_3(SO_4)_2.¼H_2O$, a compound with ~3 atom% H [41], while the structural characterization of the deuterated form of the ERS-7 zeolitic framework was achieved using simultaneous refinement of XPD and NPD [42]. In a significant extension of capabilities, a combination of synchrotron XRD and neutron methods has allowed the *ab initio* structural solution of the deuterated version of the framework structure of $Ga_2(HPO_3)_3.4H_2O$ (with 29 atoms in the asymmetric unit cell, 117 refineable structural parameters) – a powerful example of the amount of information that can be retrieved when using these two complementary techniques [43].

2.3 The characteristics of neutron sources

There are two main types of neutron source used for condensed matter studies: steady state (usually reactor) sources and pulsed (usually spallation) sources [10].

2.3.1 Reactor sources

Nuclear reactors are traditional "steady state" neutron sources. A typical research reactor operates with a highly U-235 enriched uranium fuel core surrounded by a moderating region, typically the fuel-moderator region being around 2.5m in diameter. The production of neutrons is by fission, one of the major products of such reactions being neutrons. The moderating region, typically of light or heavy water, also provides the coolant region for the core. This is surrounded by a reflector region, typically of beryllium and water, which reflects back fast neutrons that will induce further fission processes. The initial biological shielding is then provided by a concrete-enclosed "swimming pool" of water in which the reactor pressure vessel sits.

The beam tubes come from the reflector region and high neutron fluxes can be obtained by optimising this set-up. Thermal neutrons are obtained from water moderators at around 300 K, which give a peak in the Maxwellian flux distribution at around 1.2 Å. The available neutrons from a reactor source can also be tuned by using different moderator materials, yielding a different flux profile. Thus hot sources can be constructed, for example at the ILL high flux reactor in Grenoble [44] the hot source is of graphite at 2400 K, enhancing the neutron flux at wavelengths less than 0.8 Å. Similarly, cold sources typically use liquid deuterium at 25 K, providing enhanced flux at wavelengths of greater than 3 Å. Wavelength

selection for particular experiments is achieved by means of crystal or multilayer monochromators or by choppers. The neutrons produced by any of the sources can be transmitted to the experimental areas either by normal beam tubes or by neutron guides (typically of metal multilayer supermirrors or of a substrate material coated by ^{58}Ni), designed to minimise neutron absorption and hence to maximise the transmitted flux. There has been a recent renaissance in the technology of neutron guides and associated optics both at reactors and spallation sources, and dramatic increases in flux at the sample position are possible using this technology [45], particularly for the colder (longer wavelength) neutrons so often used in biological studies where intermediate diffraction resolutions are accessed (typically 1.5 to 2.5 Å).

Fission-based neutron production is a high power process - the Oak Ridge high flux isotope reactor [46] operates at a power of 85 MW in cycles of around 22 days. The Oak Ridge reactor, however, is not entirely dedicated to neutron production, a significant aspect of the design of the core being to optimise production of the desired isotopes. The ILL high flux reactor, at 58 MW, is dedicated to neutron production for condensed matter and other, more fundamental, experiments using neutrons. The ILL reactor cycle is around 50 days between fuel element changes.

2.3.2 Spallation sources

The characteristics of a pulsed spallation source are very different to those of a reactor neutron source. The production mechanism itself is a dynamic process, being based on an accelerator rather than a steady state reactor. The word “spallation” comes from a mining term meaning to chip, evoking visions of an impact mechanism for neutron production in such sources. This is more-or-less the case. Charged particles are accelerated to high velocities (energies) in the accelerator before being fired at a heavy metal target. The consequent impacts induce nuclear processes that produce neutrons (typically tens of neutrons for each incident accelerated particle). As this method is less well known we will give here a more detailed account of the neutron production process at ISIS, the spallation neutron source at Rutherford Appleton Laboratory in Oxfordshire, UK [47].

The production of particles energetic enough to lead to efficient spallation involves three stages. First, an ion source produces H^- ions which are accelerated in a pre-injector column to 665 keV. In the linear accelerator, the second stage, the H^- ions pass through four accelerating radio frequency cavities to reach an energy of 70 MeV. At injection into the third acceleration stage, the synchrotron, the electrons are stripped from the H^- ions by a very thin (0.25 mm) alumina foil, producing a circulating beam of protons.

The proton synchrotron, of 52 m diameter, accelerates 2.5 x 10^{13} protons per pulse to 800 MeV, before they are extracted and sent to two target stations where the neutrons are generated. This process is then repeated 50 times a second. At ISIS four pulses in five are extracted to the original target (TS1), while one pulse in five is directed towards the new second target station (TS2), which thus operates at a frequency of 10Hz. The spallation target is made from a heavy metal such as depleted uranium, tantalum or tungsten. The highly energetic protons produce neutrons by chipping nuclear fragments from the heavy metal nucleus. For an 800 MeV proton beam some 15 neutrons are typically produced by each proton hitting a tantalum target.

Around the target there is an array of small hydrogenous moderators to slow down the neutrons to thermal or close to thermal energies. There are three moderators at ISIS TS1: one at ambient temperature (316 K, H_2O), one of liquid methane (100 K, CH_4) and the cold moderator of liquid hydrogen (20 K, H_2). To preserve the sharpness of the initial 0.4 μs neutron pulse, the ISIS TS1 moderators are small (typically 10x10x5 cm^3). The resultant under-moderation gives a rich epithermal component to the spectrum, with a high flux of high energy, short wavelength, neutrons. The second target (TS2) is optimised for the production of colder neutrons, their generation enabled by three cold moderators (two coupled moderators – hydrogen and methane – offering broad pulse structure and one decoupled methane moderator), and their use facilitated by the low repetition rate that allows for longer data collection frames (using time-of-flight methods [10]). The characteristics of the neutrons produced by a pulsed spallation source such as ISIS are significantly different from those produced at a reactor. This not only means that neutron scattering experiments are carried out in different ways (using time-of-flight methods), but also leads in some cases to applications in different scientific areas to those accessible on a reactor source.

2.3.3 Current and future developments of sources

There are still only a few intense spallation neutron sources operating for condensed matter research, although there exist many plans for future sources both on a national scale, with performance matching that of present sources, and on an international scale, with substantially enhanced performance. For reference, the power dissipated in the high power target (TS1) of ISIS is 160 kW, and that of the more recently commissioned US Spallation Neutron Source 1.4 MW, to be contrasted with the 58 MW of the ILL High Flux Reactor.

For reactors, large performance improvements for neutron scattering experiments are available from improved neutronics (including guides and other in-beam optics) and from enhanced detectors (see below). Thus modern research reactors such as the recently commissioned FRM-II (Munich; [48]) and OPAL (Lucas Heights, Australia; [49]), although operating at 20 MW power, promise highly competitive count rates for many experiments. Future plans for expansion in the area of spallation sources are extensive, capitalising on the fact that the current specification for such sources is not yet close to the technical limit. On both the accelerator and target station side, advancing technology allied with increasing experience of operating such sources promises a rich future. The ISIS second target station (TS2) offers a source optimised for cold neutrons operating with one pulse in five from the current ISIS accelerator – a 10 Hz source. The moderators on TS2 optimise wavelength, flux and pulse width characteristics in the cold neutron (longer wavelength) region, while still offering good flux at shorter wavelengths. On the accelerator side, there are 1 MW sources in operation in the USA (SNS, Oak Ridge, Tennessee; 1.4 MW [50]) and in Japan (the Materials and Life Science Facility MLF at the J-PARC complex, Tokai; [51]). For still higher flux, the ESS, the European Spallation Source to be sited in Lund, Sweden, will provide a long pulse 5 MW source [52].

2.3.4 New opportunities: enhanced neutron powder diffraction instrumentation

There has been a dramatic enhancement of the capabilities of neutron powder diffractometers over the past few years, making these valuable experiments available to a wider range of applications. The improvements in instrumentation have allowed neutron powder diffraction to move towards new areas of application such as those described in this review. These improvements have focused around the combination of very high flux, coupled with high resolution, allowing reflection intensities to be utilised most effectively in a profile fitting method over a large *d*-spacing range. These factors are of particular value in the present context as, in combination, they offer improvements in the peak-to-background ratio and the potentially poor signal-to-noise ratio due to the incoherent scattering of the hydrogen atoms; the instrumental resolution also effectively dictates the complexity of structure that can be successfully analysed [53], which is of particular importance in potential studies of molecular systems discussed here.

The first criterion is met using the new generation of high-flux neutron sources. The second is resolved on steady state source instruments such as D20 [Figure 2; 54] and WOMBAT [55] by using a high take-off angle configuration (utilising a Ge(115) cut-surface, single crystal monochromator) where high flux is coupled with resolution sufficient to allow the study of materials with larger asymmetric unit cell volumes,

up to at least 1000 Å^3. Instruments on time-of-flight (t-o-f) sources (such as GEM at ISIS [Figure 2; 56]) optimise resolution in a different way, by using a combination of instrument flight path and high scattering angle detector arrays (or in the case of POWGEN [57], a continuous angular coverage detector array). The potential in this area of instruments that are optimised for diffraction under extreme conditions should also be noted, for example the PLANET diffractometer at J-PARC offers the capability for powder diffraction at high pressure for the study of hydrogen-containing materials, including dense minerals [58]. These instruments have the clear potential to offer suitable flux - resolution combinations for the study of hydrogenous powders (see, for example, the PND study of $Li_4BH_4(NH_2)_3$ using GEM [40]). However, wavelength- and sample-dependent attenuation corrections can add complications in fitting diffraction intensities across the full range of neutron energies in these data [37], and this must be taken into account in tackling experiments on highly hydrogenous materials.

Figure 2 – the high flux neutron powder diffractometers D20 at ILL (left) and GEM at ISIS (right)

2.4 Initial technical assessments of the potential for NPD study of hydrogenous materials

A series of detailed technical assessments have been carried out to establish the potential of neutron powder diffraction in the study of highly hydrogenous systems, in terms of sample characteristics, typical counting times and quality of the resulting data. These are detailed elsewhere [59], but summarised briefly here. This work has focused on both empirical and analytical approaches, the philosophy being that application of these methods requires that the practical implementation of the technique in real systems must be developed in parallel with technical advances, particularly if these methods are to be more widely adopted by a range of users of neutron facilities. These technical assessments have indicated the following:

- Attenuation of the beam, through absorption, incoherent scattering and multiple scattering effects at wavelengths between 1.3 and 1.9 Å, for samples up to 2.5 cm^3 with moderate hydrogen content (33 atom%), has been found to be negligible [59];
- Although sample sizes are, in part, dependent on hydrogen content and crystallographic complexity, as an indication, a typical high-quality data set from samples with 35–40 atom% hydrogen requires ~1 hr of data collection for a 2 g sample on D20;
- Lower quality data sets which are still usable in constrained refinements can be collected in 10 mins on 2 g samples or 4 hrs on ~100 mg;

- For samples having higher hydrogen contents, such as clathrates and hydrides (~65–75 atom% H), theory predicts that annular sample cans should be employed, as used for materials with high beam attenuation. However, recent direct measurements on methane clathrate in annular and 5 mm vanadium cans do not support this hypothesis [60]. Such discrepancies could be due to the low packing densities of powders compared to ideal single crystal densities that are used in the calculations [61]. As powdering the sample will often reduce the density to less than 70% of the ideal single crystal value, the effect is similar to diluting a strongly absorbing or incoherently scattering sample with a matrix;
- In many hydrogenous materials the relatively large thermal motion of the light hydrogen atom means that the main contribution from hydrogen to the Bragg peaks in the neutron scattering profile is found in the longer *d*-spacing (lower 2θ) reflections;
- Due to the large thermal motion of hydrogen and associated increase in inelastic scattering of neutrons at high temperatures the background in powder diffraction data sets increases markedly with increasing temperature; this is particularly so for molecular species. This sloping background, decreasing towards smaller *d*-spacings, becomes more difficult to define in regions of overlapping reflections making it difficult to define displacement parameters and correlated structural parameters. In a recent study of synthetic gibbsite by neutron powder diffraction at SINQ [62], the refined hydrogen positions would not converge even while using soft constraints This is likely due to the high temperature of data collection (RT to 400 °C) increasing the effect of the hydrogen thermal motion, stressing the importance of cooling samples wherever possible to improve not only overall data quality but also the relative contributions of the H atoms;
- The experimental set-up can also be optimised to extract the maximum information from the region in which the hydrogen scattering has most effect, by tuning the wavelength of the data collection or collecting data at different wavelengths, or by employing a variable count regime, with longer counting times in the most relevant regions of the pattern;
- We have determined that the incoherent contribution of the neutron scattering from the ^{1}H isotope for a single wavelength incident beam is isotropic, and (depending on detector stability) varies sufficiently smoothly with scattering angle to be normally easily modelled using standard profile fits, or reliably subtracted from the data. As noted previously the exceptions are systems where there is large thermal motion of hydrogen in structurally complex compounds. In the majority of the diffraction patterns examined in these assessments, the backgrounds are

modelled in the GSAS [63] package by standard methods using a Chebyshev polynomial profile with 4-9 parameters;

- The capability of carrying out *in situ* experiments is a crucial advantage of neutron diffraction, the ability of neutron radiation to penetrate deeply into matter making it especially suited to the study of real-time behaviour of bulk functional materials, including humidity controlled sample chambers and gas flow apparatus. The use of non-isotopically enriched samples makes many experiments (such as *in situ* dehydration experiments in air) far more accessible, and this has been established in a range of *in situ* studies of hydrogenous materials (see below);
- The importance of exploiting refinement against multiple data sets has become increasingly apparent in this work. Simultaneous refinement of SXD and NPD data can allow excellent resolution of hydrogen positions, as described for the structural refinement of $Cs_2C_2O_4.H_2O$ [39]. Single crystal data provide more precise information about the positions of the heavy atoms in the structure, which can then be fixed in subsequent refinements of hydrogen positions against NPD data. This results in a considerable reduction in the number of refineable parameters thus allowing specific information on the hydrogen positions to be extracted. Alternatively the structural model can be refined in an unconstrained manner against both SXD and NPD data; using different weights on the various data sets can allow the refinement to focus on extraction of accurate hydrogen positions by assigning the neutron data a higher weight.

3. Examples of Applications of NPD in the study of Hydrogenous Molecular Systems

As noted above, structure solution of organic compounds by SXD is generally considered routine and due to the presence of only light atoms in the structures, important hydrogen atoms can usually be directly observed from X-ray Fourier maps. This has been seen in some of the examples of X-ray diffraction experiments carried out under multiple conditions quoted above, and in a fine example in the study of pharmaceutical materials, the study on solvated crystalline forms of tetroxoprim [64]. In many of these cases, the positions of the most relevant hydrogen atoms were obtained unambiguously from the Fourier analysis and could be subsequently constrained and refined. In cases where single crystals are not available, there is strong evidence that, with modern X-ray powder diffractometers, including those at synchrotrons, powder diffraction can provide enough information to allow structure solution from polycrystalline molecular organic materials [65, 66], and is gaining acceptance as an alternative to the traditional single crystal measurements. In an excellent example of the *ab initio* structure determination

of an organic pharmaceutical compound from powder diffraction data, the structure of the commercial diuretic chlorothiazide was solved using synchrotron radiation and variable count times [67].

However, as in many examples of molecular systems using XRPD, the structural hydrogen positions in this latter example were not refined, but placed using a 'riding model', later improved by the use of combined XPD and NPD refinement [38]. While the use of calculated H atom positions is viable in the case of geometrically standard hydrogen atom containing groups, where more unusual bonding involving hydrogen occurs, such as strong hydrogen bonds, the use of a rigid molecular geometry in the modelling of the diffraction data yields little useful information on the true hydrogen position. However this is often an important reason for studying the crystal structure – for example in studies of polymorphism where different hydrogen bonding patterns occur, or in cases of proton migration or transfer. Furthermore in such cases deuteration, even when chemically feasible, may change the hydrogen bonded network and its behaviour with changing conditions; this emphasises the need for neutron powder diffraction of hydrogenous materials as a viable alternative approach.

3.1 Thermochromic phase transition in Squaric acid-bipyridine

A powerful example of hydrogen determination from neutron powder diffraction data of an organic compound is given by the rapid data collection on the 1:1 adduct formed of squaric acid and 4,4'-bipyridine (Figure 3), containing approximately 33 atom % H, and investigated as a model for potential proton transfer [68]. The long, thin, plate-like crystals were unsuitable for single crystal neutron experiments and H positions could not be extracted from the SXD investigation of the high temperature form II phase at 453 K. Neutron powder diffraction patterns collected on D20 in high-resolution mode, however, allowed the satisfactory refinement of the structure (Figure 4), giving crucial information on the hydrogen bonding in the high-temperature form II polymorph of the compound. This was achieved in spite of the relatively short data collection time (60 mins) and the small sample size used (0.75 g). Structural optimisation of Form II by computational methods confirmed the refined structure to represent a stable point on the potential energy surface.

Figure 3 – the thermochromic phase transition in 1:1 squaric acid:4,4'-bipyridine is due to proton transfer and has been characterised by a range of techiques including NPD.

Figure 4 – high quality NPD data and good quality Rietveld fits were obtained for both polymorphs of 1:1 squaric acid:4,4'-bipyridine.

3.2 Polymorphism and proton transfer in molecular complexes

An example of the use of NPD in the area of polymorphism is provided by the study of the two polymorphs of the 2:1 molecular complex of isonicotinamide and oxalic acid (IN_2-OA). Previous X-ray and computational studies of this system had shown the existence of two polymorphs, which show a distinct conformational difference, the oxalic acid moiety being oriented in a "*cis*" conformation in form I and a "*trans*" conformation in form II [69]. A combination of high resolution X-ray diffraction, single crystal neutron diffraction, charge density and computational approaches established not only the accurate structures of the two forms, but also indicated the energy difference between the polymorphs [69, 16].

Figure 5 – The two polymorphs of IN_2-OA exhibit "cis" (Form I, top) and "trans" (Form II, bottom) conformation of the oxalic acid with respect to the isonicotinamide.

NPD was thus undertaken on these forms [70] as part of the programme establishing the potential of the technique in the study of hydrogenous molecular systems, since the presence of a short, strong hydrogen bond in the system, and its potential as a possible proton transfer system rendered the accurate determination of the crucial hydrogen atom in the short, strong hydrogen bond (SSHB) important. Experiments were carried out on D20 at ILL, and the structural parameters were refined using various models for analysing the combined data. The "target" parameters were established by the single crystal neutron study, giving the elongated O–H covalent bond length within the SSHB at 1.161(3) Å. Refinements were carried out in the following ways: refinement of NPD using the heavy atoms from the single crystal X-ray structure; unrestrained joint refinement of the NPD and single crystal X-ray data; restrained joint refinement of the NPD and single crystal X-ray data, with the bond length restraints based on the X-ray determined parameters for the non-hydrogen atoms. Fourier reconstructions of the hydrogen atom in the short hydrogen bond were also evaluated (Figure 6).

Figure 6 – Refined bond lengths to H atoms (left) and Fourier map in the region of the strong hydrogen bond (right), from the combined neutron-X-ray refinement of Form I of IN_2-OA.

In all cases a reasonable determination of the crucial O–H bond length (1.173(18) Å in the combined refinement) was obtained. This would be inaccessible through the use of geometrically calculated H atom positions, and the use of the complementary NPD data plays a vital role in allowing this determination. Fourier difference map resulting from the joint refinements illustrates a very well localised density corresponding to the hydrogen atom – the density map calculated with a weighting that emphasises the contribution of the neutron data. The overall profile fit for the NPD data from the refined model is of good quality (Figure 7).

Figure 7 – Rietveld fit for the NPD data, with the model resulting from the combined refinement of Form I of IN_2-OA.

The refinement of the form II structure using the same models shows very similar results (Figure 8), and importantly the fact that the nature of the SSHB is different in this case (the HB shows a far more centred proton, with O-H distance 1.253(15) Å) is maintained in the NPD-driven study, and although the agreement between the NPD and X-ray determined distances is not so close in this case, the NPD is in good agreement with the SCND distance of 1.235(5) Å; this emphasises the difficulty in using X-rays to determine H positions in close-to-centred short hydrogen bonds.

Figure 8 – Refined bond lengths to H atoms (left) and Fourier map in the region of the strong hydrogen bond (right), from the combined neutron-X-ray refinement of Form II of IN_2-OA.

A similar study of the proton transfer and polymorphism in lutidine-pentachlorophenol (PCP) complexes has also yielded similarly promising results, while indicating some of the limits in trying to apply NPD in such complex molecular systems [70]. These hydrogen-bonded molecular complexes again contain SSHBs, and the position of the proton can be tuned by altering the chemistry of the complex (pK_a-mediated proton transfer) or by changing external conditions such as temperature. The lutidine-PCP system [71] includes several complexes and polymorphs for which it is challenging to grow even X-ray sized single crystals but for which neutron data are vital. Initial studies on exemplar complexes were thus carried out on D20 (Figure 9). The resulting joint NPD-SCXD refinements of the structures of the PCP:2,6 lutidine and PCP:2,4-lutidine complexes (Figure 10) show very similar results to those found for the IN-OA complex, with a very accurate determination of the (elongated) O–H covalent bond length in the SSHB in the 2,6 complex (1.082(16) Å) and for the elongated N–H covalent bond length in the 2,4 complex

(1.063(16) Å), in which proton transfer has taken place. In both cases there is a well localised H atom peak in the Fourier difference map. This accurate determination of the hydrogen parameters by combined X & n data offers the potential to carry out the necessary comprehensive and chemically-relevant studies of such systems, including future variable temperature (VT) work.

Figure 9 – Typical Rietveld fit from D20 study of PCP-lutidine complexes, specifically for the 2,4-lutidine complex.

Figure 10 – Refined bond lengths toselected H atoms (left) and Fourier map in the region of the strong hydrogen bond (right), from the combined neutron-X-ray refinement of PCP:2,6-lutidine (top) and PCP:2,4-lutidine (bottom).

The study of the PCP-lutidine complexes has also given an indication of the current limits of such studies in terms of molecular complexity. The complex of PCP and 3,5 lutidine produces a structure with a total of eight molecules in the asymmetric unit (Figure 11, left), and while the diffraction pattern was of reasonable quality (Figure 11, right), this was found to be intractable to refinement by NPD, even in a joint refinement with SCXD data

Figure 11 – The NPD study of the PCP:3,5-lutidine complex with a large asymmetric unit containing multiple molecules proved not to be able to yield an adequate structural refinement.

3.3 Hydrogen location, hydrogen bonding and structural evolution in molecular systems

Hydrogen bonding is the key interaction that defines the crystal structures of many biochemically important small organic molecules such as sugars and amino acids. To demonstrate the applicability of NPD to such systems we have studied some simple amino acids. Diffraction data were collected for typically 45 mins on a 3 g sample of the N-methylated amino acid sarcosine at 120 K on D20. These data were analysed using profile refinement with no constraints on the atomic positions (13 atoms, 39 coordinates, two global ADPs used for hydrogen atoms and for carbon, oxygen and nitrogen). The two strong hydrogen bonds are well defined and show the expected lengthening of the N–H bond (to 1.06(2) Å) for the strong hydrogen bonded interaction, compared with that in the weaker, more conventional hydrogen bond in which the N–H covalent bond is of “normal” length (0.95(2) Å). Interestingly, the original single crystal X-ray study had yielded N–H distances that were equal at 0.99 Å [72].

The rapidity of NPD data collection also means that variable temperature studies on this type of system become feasible. Data collected from glycine heated from 115 K to 430 K over a 6 hr period have been analysed to define the changes that occur in the hydrogen bonded network (Figure 12). These show evidence of a correlation between the hydrogen atom geometry (which have never previously been elucidated) and the trends in the lattice parameters (an anomaly in the *c*-axis, which was previously known from XRPD). In glycine rotation of the molecules relative to each other between 300 and 350 K cause a bifurcated hydrogen bond to become essentially a single hydrogen bond. Such a level of geometric information is only accessible from rapid-scanning powder data and has clear implications for the use of the technique in studying structural evolution and phase transitions in molecular systems.

Figure 12 – Variable temperature neutron powder diffraction of glycine allows structural trends between molecular geometry (N-H1 distance, right) and unit cell parameters (c – left) to be correlated.

Many saccharides, including di-, tri- and poly-saccharide forms and their hydrated derivatives, are important excipients in the formulation and processing of pharmaceuticals [73], and understanding their hydration behaviour is thus highly relevant in their application as filler-binders in tablets and solid form inhalers where hydration and dissolution factors control tablet and particle disintegration rates. The relevance of *in situ* studies of such materials during thermal or humidity changes has been discussed recently [74, 75, 76, 77], and while information on phase stability and changes as a result of heating or cooling or relative humidity can be obtained using powder X-ray diffraction, this has drawbacks as it samples mainly the surface of a polycrystalline mixture, a limitation of particular concern when investigating the phase and reaction chemistry of a pharma-compound as a function of particle size – a key parameter in controlling dissolution rates. We have used NPD to study the *in situ* hydration of α-lactose (one with good crystallinity, the other with small particle sizes of 0.1-1 μm) and trehalose (with good crystallinity), providing information on the kinetics of these hydration processes for the bulk polycrystalline material. The experiments were carried out on D20, with a typical scan following the course of the hydration taking around 4-6 hours in total (Figure 13).

Figure 13 – Stacked plot viewed down the intensity direction showing the evolution of the diffraction patterns of standard stable α-lactose as a function of time in 100% relative humidity at 45°C; the positions of three strong reflections from α-lactose monohydrate are shown.

For α-lactose a simple hydration process occurs, which is consistent with the simple growth of dihydrate from the crystallite surface and this process occurs more rapidly to completion for smaller crystallite sizes (Figure 14). On the other hand, a more complex mechanism seems to be involved in the formation of an intermediate hydrated phase of trehalose *en route* to its dihydrate. This ability to observe pharmaceutical compounds *in situ* in controlled humidity and temperature conditions and study bulk material rather than surfaces is of considerable relevance to production and the storage of many active pharmaceutical compounds, and the *in situ* NPD technique accessible to hydrogenous materials could also readily be applied to complex formulations and those in pelletized forms.

Figure 14 – Phase percentage of α-lactose monohydrate as a function of time in highly crystalline (black filled circles) and small particle size (grey filled circles) forms.

The ability of NPD to reveal previously undetermined phases is also illustrated in the recent study of *cis*-platin [78]. Cisplatin is the single most well-recognised and successful chemotherapeutic drug used today for the treatment of testicular and ovarian cancers [79, 80]. In order to model interactions of active drug molecules with biological targets, full and accurate definition of the structures of these molecules is essential, but while many drug molecules have been examined in this way, but until now cisplatin has been perhaps the most prominent for which full structural information has, until recently, been unavailable. A low resolution crystal structure was available for the α-polymorph [81], but the structure of the administered form (β) was unknown, and the relationships and transformations between the two polymorphs were also not known. Given the current prominence of studies of polymorphism and the influential effect this phenomenon is known to have on the delivery and function of pharmaceuticals, and the importance of understanding the relative stability of polymorphs and the structural transitions between the solid forms, the lack of structural information on these polymorphs was a clear anomaly, which was addressed by the use of NPD to provide high resolution crystal structures of both crystalline polymorphs, showing both hydrogen positions and inter-molecular hydrogen bonding, and demonstrating how polymorphic inter-conversion occurs over different thermal regimes.

To obtain a complete description of the structures of the two polymorphs, including hydrogen positions, the powerful combination of SCXD and NPD was used, with the SCXD used to determine accurately the atomic coordinates of the non-hydrogen atoms, while Fourier analysis of the NPD data allowed resolution of the orientations of the NH_3 groups in the crystals. The yellow crystals of the beta form were found to

transform to the alpha form at low temperatures, so while the measurements of the alpha form were conducted at 100 K, data on the beta form were collected at 220 K. Both forms are found to be triclinic, and both refinements resulted in realistic N-H distances and angles (average N-H bond distance = 1.00(5) Å, average H-N-H angle = 107(7)°). Figure 15 shows the alternating arrangement of the NH_3 groups and the Cl atoms in each stack of square planar molecules along the *c* axis. In both forms, the central Pt atoms appear staggered along *c*, with a Pt-Pt-Pt angle of ~170° for the alpha form, compared to ~160° for the beta form. It is likely the structure adopts this lower-energy conformation (rather than a perfectly stacked arrangement of Pt atoms) as a result of the orientation of the pyramidal NH_3 groups. Hydrogen bonding plays an important role in the packing of the cisplatin molecules in the solid state, with the orientations of the NH_3 groups playing an important role in this.

Figure 15 – the transformation between the crystalline forms of cisplatin: (left) the structure of the alpha form showing the layers of molecules in the ab plane (top) and highlighting the H-bonding (dashed blue lines) between the layers along c (bottom); (centre) the overlaid unit cells of the alpha and beta forms, showing the transformation under heating from the low T alpha form (blue) to the high T beta form (red); (right) the structure of the beta form, showing the layers in the ab plane (top) and showing the H-bonding between the layers along c (bottom).

To determine the important thermal stability properties of the two forms of cisplatin, the relative stability of the two polymorphs with respect to temperature was examined via *in situ* variable temperature NPD experiments. A ~2 g sample of polycrystalline beta cisplatin at room temperature (RT) was initially cooled to 100 K, then heated to 360 K, and finally returned to RT at a fixed rate of ~1.5 deg.min^{-1}. These scans yielded good quality NPD data from this fully hydrogenous sample. Sequential refinement of the relative phase fractions using rigid body models of the structures of the two enantiotropic polymorphs (based on those previously refined using the combined SXD and NPD data) showed a distinct transformation from the initial beta form at RT to the pure alpha form below 200 K, over a temperature range of ~70 K. On heating, the beta form does not begin to appear until temperatures above ~310 K are reached, with the almost pure beta form re-emerging at ~350 K, while as the sample was returned to RT, the beta form remained the dominant phase. The unexpectedly large degree of hysteresis apparent in the phase transition temperatures (approximately 120 K; 78) between the temperatures of formation of the slightly denser alpha form upon cooling and the reversion to the beta form is suggestive of thermodynamic stability of the alpha form at ambient temperatures. This can be explained by examining the structural mechanism of the phase transition, which involves a colossal, reversible rearrangement of cisplatin molecules and the stability of the alpha phase is related to the large activation barrier for the transformation to the beta phase.

3.4 Temperature-dependent proton disorder in dimeric systems

As an example of an ambitious study which pushed beyond the limits of what is currently feasible, we highlight here an extensive variable temperature study intended to examine proton disorder within the pair of hydrogen bonds in a carboxylic acid dimer system. This well-studied phenomenon has been characterized extensively by single crystal neutron diffraction in systems for which it has been possible to prepare large single crystals [19, 82], but in others only X-ray sized single crystals have been available, including the material of interest in this study, 2,4,6-trimethylbenzoic acid.

Many derivatives of benzoic acid (BA) crystallise as hydrogen bonded dimers, and dynamic double proton transfer within the hydrogen bonds allows swapping between two tautomeric forms [83]. In the crystal structure, this is manifest as disorder of the hydrogen-bonded hydrogen atom over two sites. In this disorder model there are two minima, corresponding to two dimer configurations, A and B, that are identical in energy in the gaseous state but have slightly different energies due to the effect of the asymmetric crystalline environment. This effect is probably so pronounced in these small dimeric systems because the local environment around the two possible hydrogen atom positions can appear very similar and hence results in a small energy difference between the two possible configurations. Earlier X-ray measurements of TMBA [84] had provided evidence for the presence of hydrogen atom disorder both from the C-O/C=O bond lengths being “almost equal” in length and from Difference Fourier syntheses. Interestingly, an earlier determination of this structure had found an almost equivalent C-O/C=O bond length distribution but had concluded that this implied the hydrogen atom was localised on a single site [85], indicating the ambiguities possible in the absence of direct observation of disorder phenomena, and prompting the previous successful investigation by variable temperature X-ray methods [28] and the present NPD investigation.

The temperature range of interest in these studies, in which the site occupancy variation of the two possible H atom sites is observed, is below 300 K, and the NPD experiments were thus carried out on D20 in the range 10-300 K, collecting data in two fashions: first, a continuous “thermodiffractometry” scan from 30-300 K with a temperature ramp of 3° per minute, with the entire scan occupying a data collection time of around 90 minutes; and secondly, full data collections of *ca.* 1 hour duration at 10, 30, 100, 170, 240 and 290 K, the temperatures being chosen to match the availability of complementary single crystal X-ray data at the last four temperatures. The evolution of the diffraction pattern in the

thermodiffractometry experiment is shown in Figure 16 (top), with the data from the full data collections in Figure 16 (bottom).

Figure 16 – NPD pattern evolution in the thermodiffractometry experiment (top) and individual diffraction patterns (bottom) from the D20 experiment on 2,4,6-trimethylbenzoic acid.

In spite of the apparently reasonable quality of the raw diffraction data, there are some problems apparent with both the data (an unexpected background shape, Figure 16, bottom) and in the refined structures. The refinements were carried out against the NPD data, using a range of strategies: refinement against PND data only; refine H against PND, fixing non H parameters (xyz, ADPs) to single crystal X-ray data values; joint refinement against PND and SCXD; joint refinement against PND and SCXD but taking into account systematic differences in H parameters from neutron and X-rays: X–H (X-ray) ~X–H (neutron) – 0.1 Å; X–X–H (X-ray) ~ X–X–H (neutron). Refinements were also carried out using a range of soft restraints ion the C–H bond parameters.

Although it was possible to refine the core structure in various refinement models, accurate determination of the key hydrogen atoms parameters in the regions of interest – the carboxylic acid dimer hydrogen bonds – were unsuccessful at all but the lowest temperatures. The O–H bond length in the regions where the H atom is essentially fully localised on the major site were successful, with values of 1.048(29) and 1.034(30) Å determined at 10 and 30 K, respectively; this represents a significant success, as there are no matching SCXD data at these very low temperatures. However, in the region in which the hydrogen disorder is apparent, the determinations of the O–H bond length were less reliable and did not show a trend in agreement with previous determinations or the known ordering model. More significantly, the Fourier maps calculated to allow imaging of the dimer H atoms by structure factor calculation omitting the H atom of interest show, at all temperatures, either a single peak or a relatively noisy map (Figure 17) , and were thus inconclusive.

Figure 17 – Fourier maps in the region of the carboxylic acid dimer in 2,4,6-trimethylbenzoic acid with the hydrogen atoms removed. The inconclusive map from the NPD data (left) can be compared with the clear indication of disordered H atom density from the single crystal X-ray study (right).

It appears that in this case the ability of NPD to offer the accurate ability to resolve disordered H atoms in molecular systems has not been proven, and further work would be required to try to establish this feature. Similar findings are reported below for a non-molecular system.

4. Examples of Applications of NPD in the study of Hydrogenous Mineral Systems

4.1 Gypsum

As an early exemplar of the utility of NPD in studying inorganic hydrogenous systems, the mineral gypsum was chosen. The most common sulphate-based mineral in the world, the water content in gypsum and its variation as a function of temperature drive the properties and therefore understanding of the role of hydrogen in the structure is key. The structure of gypsum is formed from layers of CaO_8 polyhedra consisting of zig-zag chains bound by similar zig-zag chains of SO_4^{2-} units (Figure 18). These double-sheet polyhedral layers are linked by an O(1) - H(2) hydrogen bond. Prior to the study described here, only single crystal neutron diffraction data had been able to provide sufficient quality data to allow this understanding. The unit cell volume of around 500 $Å^3$ and monoclinic space group (*C*2/*c*) are sufficiently complex to provide a realistic test of the NPD technique for hydrogenous systems.

Figure 18 – the C2/c crystal structure of gypsum showing the layers linked by hydrogen bonding.

As an exemplar study, both hydrogenous and deuterated samples were studied; the refinements were carried out in both space-group settings *I*2/*a* and *C*2/*c*, and anisotropic atomic displacement parameters (ADPs) were refined in all cases [59]. In all cases the refined atomic positions compared well with those from the previous single crystal and powder studies on both the hydrogenous and deuterated materials; in particular the positions and standard uncertainties for the powder data on the hydrogenated and deuterated materials are in good agreement showing that there is no significant isotope effect in this material and illustrating the accuracy obtainable from the NPD study of the hydrogenous system. Also of interest in this study was the use of two different instruments for the comparison: the full data were collected for 90 minutes on D20 for the hydrogenous material (Figure 19; though in fact good quality refinement was obtained for data collected in as little as 5 minutes) and ~2 hours on the upgraded POLARIS diffractometer at ISIS (350 μA-h) for the deuterated sample.

In particular, the bond lengths from the powder data refinement are 1.007(6) Å and 0.929(7) Å for O-H1 and O-H2 respectively with a bond angle of 107.2(5)°, which compare favourably with the values of 0.959(3) Å, 0.942(3) Å and 107.5(2)° from the single crystal neutron study [86] and 0.961(6) Å, 0.948(4) Å, 107.2(5)° from the powder data on the deuterated material [87]. The bond length mismatch between O-H1 and O-H2 is not unexpected, as H1 makes a stronger hydrogen bond to the framework.

Figure 19 – final Rietveld refinement profile and fit for the D20 data from hydrogenous gypsum (1.87 Å incident wavelength). The inset shows the higher Q-space region.

4.2 Zeolites

As an example of high profile mineral and mineral-related materials we present here NPD studies of the highly hydrated natural zeolite goosecreekite and the *in situ* dehydration of the natural drying agent zeolite LTA. Due to their varied and often flexible framework structures, the study of the structures of natural zeolites has led to the development and engineering of synthetic analogues for specific functionalities, including application as selective heterogeneous catalysts, water softeners, industrial adsorbents and molecular sieves (88, 89). Much can be learned about the relationship between zeolite structure and functionality by modelling the adsorption of hydrogenous species (*e.g.* water, ethanol or hydrocarbons) into the zeolite channels, and various issues with the integrity and ease of study of single crystal samples, together with the difficulty of obtaining appropriately deuterated synthetic samples, the ability to use NPD on fully hydrogenous zeolite samples is a major element in allowing the full elucidation of structure-function relationships in these systems.

As zeolites have well-established metal-oxygen distances, the structure of the host framework can be refined using soft constraints or rigid body approaches, meaning that the focus of the refinement can be the extra framework ions and any adsorbate molecules, including the often crucial water molecules and their interactions with the framework controlled by hydrogen bonding interactions. As the initial exemplar demonstrating capability in the area, NPD experiments were carried out on polycrystalline samples of the natural zeolite goosecreekite [90] ($CaAl_2Si_6O_{16}.5H_2O$) on D20, which cannot be made synthetically and for which it is not possible to grow large single crystals and which has 10 unresolved hydrogen atom positions. The refinements revealed well-determined water molecule geometries (Figure 20).

Figure 20 – the determined water structure in goosecreekite (left), and sample Rietveld fit to the NPD data (right).

These results clearly demonstrate that the Bragg contribution of the hydrogen (in the adsorbed waters) to the scattering is sufficiently well defined to allow these to be fully resolved, and this result is even more impressive given the short (1 hr) collection time.

In addition, experiments both probing a zeolite structure under heating and monitoring resulting water loss (using the reduction of the incoherent hydrogenous background) and studies under controlled humidity conditions have demonstrated the viability of tracking such changes *in-situ* using NPD of fully hydrogenous samples. Following on from initial work assessing the potential in this area within our programme (studies of thermal dehydration of mesolite), subsequent experiments using a controlled humidity set-up [91] have allowed this work to be developed further.

In the latter, Zeolite LTA (used as a commercial drying agent) was used to test the effect of humidity level on the rate of hydration. Starting with a fully dried powdered sample, it was clear that the background count level was proportional to (and can be used as a measure of) the water content in the sample. Under 100% relative humidity (RH) conditions, the background level increased steadily with time, eventually reaching a plateau after ~70 mins (Figure 21), while carrying out the same procedure at 30% RH, the background counts underwent a similar steady increase before saturating, this time taking approximately 200 mins to do so (Figure 20). The different gradients in the two cases also indicate that the adsorption is unlikely to be diffusion limited, since if it were, an initial period of "surface wetting" would be expected (which would occur at a greater rate for the sample at 100% RH), after which the gradients of both absorption curves (at 100% RH and 30% RH) would be identical.

Figure 21 – Background count level of dried zeolite LTA samples exposed to 100% RH (black curve) and 30% RH (white curve) over time, as measured in-situ. Background counts were normalised to the background level at the start of the humidity ramp.

4.3 Lead hydrogen arsenate

With attempts to image disordered protons in molecular systems using NPD indicated above as being a relatively weak aspect of the programme to date, an equivalent study was carried out in the proton order-disorder mineral system lead hydrogen arsenate, which occurs naturally as the mineral schultenite but is also easily accessible synthetically. $PbHAsO_4$ shows a paraelectric to ferroelectric $P2/c \rightarrow Pc$ phase transition, related to hydrogen ordering across a short, strong OHO hydrogen bond, which shows a strong

isotope effect (313K in $PbHAsO_4$, 435K in $PbDAsO_4$). The phase transition has previously been studied extensively by variable temperature single crystal neutron diffraction [92], and in the current study data were collected on D20 on both hydrogenous (200, 250, 300, 325 K) and deuterated (300, 400, 450 K) samples. The refinements were carried out against the PND data only.

The data are of good quality for each sample, with Figure 22 showing the 300 K data sets for comparison – the increased background for the $PbHAsO_4$ sample is clear. However, it was seen that the H (and D) parameters could be refined for both the single site high T *P*2/*c* model, and with a split site (50:50 occupancy) model for the Pc model for each material for the data sets collected above the phase transition temperatures. This ambiguous conclusion is supported by the appearance of the Fourier difference maps in the region of the short, strong HB (Figure 22, bottom), emphasising that this aspect of the potential of NPD in hydrogenous samples is as yet not established.

Figure 22 – NPD data and Rietveld fits for $PbHAsO_4$ and $PbDAsO_4$ (top), and Fourier difference maps calculated from the NPD data (bottom).

However, in a second, well-known, system that exhibits a ferroelectric phase transition with a large isotope effect, the NPD approach was found to be more successful. KDP (potassium dihydrogen phosphate) has been very extensively studied, including very high resolution neutron single crystal determinations that have revealed full details on not only the hydrogen ordering in the short, strong OHO hydrogen bond, but also on some subtle associated disorder of the oxygen positions in the hydrogen bond [93]. The hydrogen-ordering paraelectric–ferroelectric phase transition involves a symmetry reduction from $I\bar{4}2d$ to *Fdd*2, and takes place at 123 K in the hydrogenous material. As a test study, NPD was undertaken on KDP above and below the phase transition temperature and in this case it was found to be possible accurately to refine the high symmetry, single site proton geometry above the phase transition (at 125 K) and the low symmetry, split proton site below the phase transition temperature (100 K). Data were collected on D20 and the structure refined against the PND data, using the heavy atom ADPs from the single crystal data. The refined parameters in the hydrogen bond are shown in Table 1, from which it is clear that the NPD offers an accurate determination of these parameters in good agreement with previous single crystal data.

Table 1 – SXD / PND bond lengths in KDP (Å)

Bond	**SCND (I-4d2)**	**PND (I-4d2)**	**SCND (Fdd2)**	**PND (Fdd2)**

P−O(H)	1.5403(4)*	1.5423(15)	1.583(20)**	1.5798(32)
P=O			1.508(20)	1.5069(32)
O−H	1.0677(16)	1.0862(62)	1.05(14)	1.0826(43)
H· · ·O	1.4276(15)	1.4072(62)	1.43(14)	1.4224(43)

4.4 Hydrogen-containing beryllium minerals.

Many rare minerals are only available as small quantities and in polycrystalline form precluding the determination of hydrogen positions using single crystal neutron diffraction. Very high flux neutron powder diffractometers offer a route to locating definitively hydrogen positions in small quantities of a polycrystalline mineral as data of sufficient quality can still be collected in reasonable experimental times of just a few hours. Structural analysis, using neutron powder diffraction (NPD) data in combination with single-crystal X-ray diffraction (SXD) data, has been employed to determine accurately the position of hydrogen in a few hundred milligrams of two rare beryllate minerals bavenite, $Ca_4[Be_{3.5}Al_{1.0}Si_9O_{26.1}(OH)_{1.9}]$ and nabesite, $Na_2BeSi_4O_{10}\cdot 4H_2O$ [94]. Significant differences in the distribution of hydrogen atoms, as compared to that reported in the literature using SXD analysis alone, were found. For bavenite the new structural model obtained showed significant improvements on that previously presented [95]; this new structural model defined the correct fully occupied hydrogen atom position, a second partially occupied OH unit and the distribution of silicon and aluminium over the tetrahedral sites (Figure 23).

Figure 23 – overview (along b) and details of the structure of bavenite. (a) shows the environment of H2 with two weak hydrogen bonds to O3. (b) shows the environment of H1 forming two weak hydrogen bonds to O6. Be (T2) atoms within the very light gray tetrahedra, Si (T1, T5, T6) atoms within the medium gray tetrahedra, mixed Si/Al (T4) site within the dark gray tetrahedra, mixed Be/Al/Si (T3) site within the black tetrahedra with white borders, O atoms: small gray spheres, H atoms: small black spheres. H-bonds are drawn as dashed lines.

4.5 Ussingite

A number of mineral species contain very strong hydrogen bonds with O(donor)…O(acceptor) distance under 2.5 Å, and such strong hydrogen bonds are of considerable interest (see Section 3.2). It is also worth noting that hydrogen atoms in strong hydrogen bonds cannot easily be exchanged for deuterium making study of the hydrogenous mineral form unavoidable. Structural analysis of such minerals is, therefore, only possible using neutron powder diffraction methods and this technique also allows investigation of these unusual hydrogen bonds over a large temperature range. A powder neutron diffraction study of ussingite, $Na_2AlSi_3O_8(OH)$, between 4 and 850 K has been published [96]. The strong hydrogen bond in this mineral was accurately determined with the O-H distance at 1.070(8) Å and an O(donor) – O(acceptor)

separation of 2.481(5) Å at 4 K. On heating from 4 to 850 K the distribution of hydrogen along the O-O direction was found to remain asymmetric with the H atom being fully ordered at a single site, rather than partially disordered over two sites of a double-potential well, as in serandite [97]. A gradual increase in the bonded O-H distance at higher temperatures is observed, indicative of a broadening on the potential well in which the hydrogen atom is sited (Figure 24). Below 50 K, the material showed an unusual negative thermal expansion, likely to be associated with reduced bending motion of the O-H bond.

Figure 24 – the variation of the O(donor)-H and O(acceptor) H hydrogen bond lengths in ussingite as a function of temperature in the $4 \leq T \leq 850$ K range.

4.6 Pentagonite

Whilst the structure of cavansite, $Ca(VO)(Si_4O_{10})\cdot 4H_2O$, has been fully resolved with hydrogen positions through the use of single crystal X-ray diffraction, its diamorph, pentagonite, has proved a much greater challenge to conventional X-ray diffraction methods. The resolution of the hydrogen atom sites within pentagonite is therefore an excellent test of the neutron powder diffraction technique. The pentagonite structure consists of pyroxene-like chains, of composition $(SiO_3)_n$, arranged to form two-dimensional networks comprised solely of 6-ring building units. These silicate layers are linked through VO^{2+} groups (forming polyhedra with square-pyramidal geometry), resulting in a 3D structure with large pores filled with seven-coordinate Ca^{2+} and three independent water molecules (Figure 25, left). The unit cell has volume 1313 $Å^3$ and space group $Cmc2_1$. Neutron diffraction data were collected for a 400 mg sample of pentagonite on the D20 diffractometer at the ILL, Grenoble (λ=1.87 Å), at 120 K for two hours. Additionally a SXD data set was obtained for a single crystal of pentagonite, collected through the use of a Bruker-Nonius Kappa CCD diffractometer.

Simultaneous refinement against both SXD and NPD (profile fit shown in Figure 25, right) provided an excellent route for the full structural resolution of pentagonite. Six independent hydrogen atom sites were determined, including partially occupied sites (part filled water sites were confirmed to be present through thermogravimetric analysis). The geometries of the resulting water molecules are consistent with those expected, with O-H distances between 0.925-1.119 Å and H-O-H angles of 99.9-115.1°. One water molecule was found to be disordered in two possible orientations.

Figure 25 – (left) Crystal structure of pentagonite, showing the hydrogen bonding network within the pores; (right) Final Rietveld refinement profile fit for the D20 data for pentagonite at 120 K (λ=1.87 Å)

4.7 Kinoite

There has been a degree of ambiguity regarding the nature of hydrogen within the structure of kinoite since positions were suggested as part of water molecules, but were not refined [98], with unrealistic O-H distances (~1.3 Å). Infrared spectroscopy studies suggested the presence of hydrogen as part of hydroxide groups, but were unable to suggest and confirm structural positions, therefore some ambiguity remained. A neutron powder diffraction experiment is ideally suited to further probe the structure of this mineral, finally resolving the structural ambiguity regarding hydrogen atom positions.

The structure of kinoite consists of infinite, slightly undulating, chains of edge-sharing CuO_5 square-based pyramids. These chains are linked to form 2D layers, in the *ac*-plane, through Si_3O_{10} tritetrahedral units, with the central silicate tetrahedron bridging the two apical CuO_5 oxygen and the two terminal SiO_4 tetrahedra forming an edge between CuO_5 units (Figure 26). It has the $P2_1/m$ space group, with dimensions a=6.991(2) b=12.884(3) c=5.655(2), β=96.18(3)°. A joint SXD-NPD refinement was undertaken, with quality SXD data collected on a Bruker-Nonius Kappa CCD diffractometer, whilst NPD data were obtained for a powdered sample of kinoite (100 mg, minor impurities) on the D20 diffractometer at the ILL, Grenoble (λ=1.87 Å), at 120 K for two hours. Two hydrogen atom sites were resolved by this method, one as an OH group in the terminal SiO_4 tetrahedra of the tri-silicate units, with the hydrogen atom orientated towards neighbouring layers, forming a hydrogen-bonded three-dimensional network. The second hydrogen atom also formed a hydroxide group, which bridges two copper centres, with pairs of OH species forming alternate edges along the infinite copper chain, forming hydrogen bonds to silicate oxygen within the same layer. There was no evidence of water molecules within the structure during this study, confirming for the first time the nature, and structural positions, of hydrogen atoms within the kinoite structure.

Figure 26 – crystal structure of kinoite, showing the inter- and intra-layer hydrogen bonding

4.8 Babingtonite

The effect of temperature on the structures of silicate minerals containing strongly hydrogen bonded Si-OH groups is of interest as such materials can be used as models for the study of incorporation of water into feldspars as hydroxyl groups. Generally the very low level of Si-OH groups in natural feldspars results in great difficulties in directly studying these units. Babingtonite, $Ca_2Fe^{2+}Fe^{3+}Si_5O_{14}OH$, is a calcium-iron

inosilicate, whose structure consists of pairs of silicate chains, with repeat units of five silicate tetrahedra, parallel to the (110) plane. These chains are linked to form a three-dimensional framework by two pairs of edge-sharing FeO_6 octahedra, with pores in the resulting structure occupied by Ca^{2+} cations (Figure 27). The silicate chains are of the wollastonite-type, with the twisted arrangement of the chains resulting in a short O(-H)...O distance of 2.581 Å (Figure 27, inset), which when combined near linear O-H-O angle of 174.5°, is indicative of a strong hydrogen bond. The structure has the $P\bar{1}$ space group, with cell volume 346 $Å^3$.

Figure 27 – crystal structure of babingtonite with, inset, the strong hydrogen bonding environment

A phase pure sample of babingtonite (750 mg) was studied at four temperatures (100, 298, 575, 800 K, three hours each) on the D2B high resolution NPD diffractometer at the ILL, Grenoble (λ=1.59 Å). Structure refinement against NPD data alone was carried out for each temperature data set, with changes in the lattice parameters and O-H...O configuration extracted. Similar, parabolic rates of expansion were noted for all three crystallographic axes. Disregarding the 575 K data set initially, the O1...O11 distance can be observed to increase parabolically, as expected due to positive thermal expansion of all lattice parameters. This expansion has little effect on the O-H distance, which remains at approximately 0.99 Å. These two effects result in a slight increase in the O...H distance, as expected. The data collected at 575 K does not fit the trend described above, with a slight decrease in the O1...O11 distance, corresponding to a sharp decrease in the O-H, and an increase in the O...H distances (Figure 28). This effect is as a result of changes in the Si-O-Si angles within the square defined by three silicate tetrahedra and the O-H...O bonding arrangement (Figure 28, inset). These angles increase at similar rates between 100 K and room temperature, therefore having little effect on the O...O distance. However, on heating to 575 K one Si-O-Si angle decreases sharply, whilst the other increases. Whilst causing the O...O distance to decrease slightly, it also has the effect of pulling apart the H...O distance, as there is little variation in the Si-O-H angle over the temperature range studied (118-120°), bringing about a decrease in the O-H distance. On further heating to 800 K, similar values are noted for both Si-O-Si angles, resulting in the higher temperature data fitting the previously described trend. From this study it is clear that NPD is an excellent tool in the study of the movement of hydrogen atoms within a strong hydrogen bond.

Figure 28 – variation in the O-H...O configuration in Babbingtonite as a function of temperature in the 100-800 K range.

5. Examples of Applications of NPD in the study of Hydrogenous Material Systems; Organometallics, hydrides, hydrates and salts

5.1 Organometallics

As a context for the following brief summary of some recent PND studies of organometallic systems, Piccoli *et al.* [99] recently noted that the cost of deuterating a complicated organometallic sample is often so prohibitive that it is seen to "outweigh the benefit of pursuing neutron powder diffraction". The optimisation of collection geometries and experimental setups, which would reduce the need for deuteration, would therefore have enormous impact on the study of organometallic hydrogenous materials. As part of our programme to establish PND as a routine tool for the study of hydrogen-containing systems, we have therefore studied a set of exemplar materials to assess the potential, including Zeise's salt and other organometallic complexes.

Zeise's salt ($KPtCl_3(C_2H_4)).H_2O$ is the archetypal example of metal-olefin complexation and has been previously studied extensively using single crystal X-ray and neutron diffraction methods, which have shown the key structural characteristics such as the strong *trans* effect of the C_2H_4 ligand on the Pt–Cl bond and the non-planar nature of the coordinated ethene ligand. In our exemplar study, NPD data were collected on D20 in 1 hr from a 1g polycrystalline sample of Zeise's salt at 120 K. A full unconstrained refinement, (using only isotropic ADPs) rapidly converged, to yield the structure shown in Figure 29. Selected extracted bond distances and angles are summarised in Table 2 and compared with the corresponding SCND data.

Figure 29 – Schematic view of the structure of Zeise's salt refined from NPD data at 120 K, showing orientation of the C_2H_4 ligand and the anisotropic nature of the H atoms.

Table 2. Selected extracted bond lengths and angles for Zeise's salt from (a) SCND at 298 K ($P2_1/c$, a = 11.212(3) Å, b = 8.424(6) Å, c = 9.696(6) Å, β = 107.52(4)°) and (b) NPD data at 120 K ($P2_1/c$, a = 11.1378(4) Å, b = 8.2444(3) Å, c = 9.4749(3) Å, β = 106.5041(23)°)

Atoms	Distance (Å)	
	SCND (298 K)	NPD (120 K)
O–H(5)	0.975(9)	1.005(13)
O–H(6)	0.940(8)	1.025(14)
C(1) –H(1)	1.096(7)	1.131(12)
C(1) –H(2)	1.087(7)	1.112(12)

C(2) –H(3)	1.079(8)	1.064(12)
C(2) – H(4)	1.086(8)	1.047(13)
H(5) ——Cl(2)	2.288(8)	2.214(11)
H(6) ——Cl(3)	2.380(8)	2.266(12)
	Bond Angle (°)	
	SND (298 K)	**NPD (120 K)**
H(5) –O–H(6)	103.6(6)	100.9(9)
Pt-Cl(2) —H(5)	103.6(2)	100.4(4)
Pt-Cl(3) —H(6)	102.5(2)	102.1(3)

For the lighter atom positions, carbon and oxygen, the standard uncertainties are comparable to those extracted from original SCXD data [100, 101] while, naturally, for hydrogen the NPD values are much superior; the C–H and O–H bond lengths are determined with a precision of ± 0.01 Å. Such data allow observation of the structural trends found previously [102], including the non-planar geometry of the C_2H_4 ligand. Cooling Zeise's salt to 120 K also results in some significant changes in certain structural parameters presumably as a result of "freezing out" of thermal motion, though it should be noted that Love's bond distance data were not corrected for the effects of thermal motion. This demonstrates another advantage of NPD over single crystal methods, in that data collections at non-ambient temperatures can be rapidly achieved so structural changes as a function of temperature can be readily monitored.

A further example of successful NPD determination of hydrogenous organometallic structures is the impressive and qualitative improvement in H atom parameters found in the study of the more heavily hydrogenous complex tetrabenzyltitanium, $Ti(CH_2C_6H_5)_4$, where once again the joint PND-SCXD approach yields a successful fit and improved structural information. Titanium complexes with alpha hydrogen atoms are systems which commonly exhibit agostic Ti....H interactions but no accurate structural data have been published previously for $Ti(CH_2C_6H_5)_4$ to determine whether a weak agostic interaction exists. In this case the unit cell volume is more than 2000 $Å^3$ in a primitive orthorhombic system, with 57 atoms in the asymmetric unit and a 50 atom-% H content. To reduce the number of parameter variables the aromatic C-H bonds were fixed but the alkyl hydrogen atoms allowed to refine freely. The improved precision in H atom parameters can be seen from the typical benzyl C-H standard uncertainties, which are reduced in the joint refinement to around 0.02 Å, compared with 0.09 Å for the X-ray data alone, while the improvement in accuracy is also evident, for example with one methylene C-H bond length determination being improved from an unrealistic value of 0.72(9) Å to a far more chemically reasonable 1.04(2) Å in the joint refinement. More significantly the titanium to α-hydrogen distances were all determined to be within the range 2.30- 2.70 Å (Figure 30), with Ti-H-M angles in the range 45-65° ; these

values compare with those found for agostic hydrogen atoms, M-H distances of 1.8-2.3 Å and M-H-M bond angle of 90-140°. This strongly supports the fact that there is no agostic interaction in $Ti(CH_2C_6H_5)_4$ between titanium and the alpha hydrogen atoms.

Figure 30 – the $Ti(CH_2C_6H_5)_4$ molecular unit showing the non-bonding (non-agostic) Ti…H distances. Ti-red, C-blue and H-grey.

5.2 Hydrides

Moving beyond these exemplars, we have also established the value of NPD in revealing important scientific trends in organometallic and metal hydride systems, harnessing the power of the developing NPD technique for hydrogen-containing systems for examining features such as structural isotope effects and temperature dependent trends, for both of which the benefits of an NPD approach are clear.

As an example of the former, a direct comparative study of Group 2 hydrides and deuterides was undertaken. These materials are of importance as potential reversible hydrogen storage materials, and typically have relatively simple crystallographic structures with high levels of hydrogen (67 atomic%). The two alkaline earth saline hydrides SrH_2 and BaH_2 were examined in this study. The full structure of the deuteride SrD_2, refined from a NPD pattern from a mixture of SrD_2 and SrND [103], was described as having one deuterium atom on a roughly symmetrical tetrahedral site, with the other deuterium atom occupying an off-centre position in the other interstitial site. NPD data were collected here for both the hydrogenous and deuterated Sr compounds on D20, with data collection times of 2 hr and 30 min for the hydride and deuteride respectively [104]. As found previously, the NPD data for SrD_2 revealed the presence of a small amount (less than 2% by weight) of SrND, which was refined as a second phase. The background of the hydrogenous material is (as expected) far higher than that of the deuteride and also included some weak additional diffuse scattering background contributions that were easily modelled in the background fitting, as part of an extensive assessment of the effect of background function choice on the refined parameters. This showed that for this simple orthorhombic structure, all background function choices that were defined using upwards of six profile parameters produced a good fit, while, importantly, changing the type of background function did not have any bearing on the refined unit cell volumes for either the hydrogenous or deuterated samples, nor did it have an appreciable effect on the refined atomic positions. As might be expected, the most significant effect was on the refined ADPs, as is well known for ADPs extracted from powder diffraction data. The best fit statistics for the diffraction data from SrH_2 and BaH_2, including modelling the weak diffuse scattering at low 2θ, were achieved when the background was

modelled using a Chebychev function. The structures were refined using no constraints on either bond lengths or angles.

The refined structural models allow a highly detailed description of the hydrogen geometry to be given, in which the H1/D1 atom occupies a close to central position in a distorted tetrahedral interstice in the Sr metal lattice (Figure 31, left), with some asymmetry in the position evident with respect to the apical Sr, while the H2/D2 atom is significantly displaced from the centre of its Sr octahedral cavity, in fact having a geometry more closely described as a distorted square-based pyramid (Figure 31, right).

Figure 31 – the H/D environments in SrH_2/D_2: (a) H1; (b) H2; (c) D1 and (d) D2. The standard uncertainly values from the NPD data for the refined Sr-Sr distances are in the range 0.00006 to 0.00011 Å and in the range 0.00004 to 0.00008 Å for the Sr-H/D distances.

For the BaH_2/D_2 structure, the D1 atom in BaD_2 again sits near the centre of the metal tetrahedral interstice, but in this case the accurate determination of the H atoms by NPD allows it to be noted that H1 atom in BaH_2 has a location that is significantly off-centre in both the x and z directions, moving towards the apical Ba atom and creating two longer Ba–H1 basal contacts (2.70 Å) and one shorter (2.46 Å). The D2 atom again occupies a slightly off centre position in the square-based pyramidal coordination environment (as seen for the SrH_2/D_2 compounds). Overall, the interatomic distances refined for SrH_2/D_2 and BaH_2/D_2 are similar to those found in ternary strontium magnesium deuterides and are typical for salt-like compounds.

As a technical development consideration, the NPD data from these hydrides were used to estimate the differences between the acquisition times required for collection of good-quality diffraction data from hydrogen-containing compounds and their corresponding deuterated analogues. Using basic statistical analysis [59] it was estimated empirically that in this case count times of order a factor of three higher would be required for the hydrogenous material in order to gain similar precision and accuracy on all parameters including the thermal factors.

To augment the study of these metal hydrides and deuterides, a full parametric variable temperature study of the structures of both the deuterated and hydrogenated forms of SrH_2 and BaH_2 was undertaken, to investigate if there are differences in the hydrogenous and deuterated structures as a function of increasing temperature. The structure refinement against the longest data set collected at 2 K for each structure was used as the starting point for the sequential (batch) refinement of the 5 min variable temperature data sets; statistical analysis showed the values of the parameters refined from the 5 min data sets were very close to those refined from the longest data sets for both the SrH_2 and SrD_2.

Accurate measurements of the unit cell parameters and fractional atomic coordinates, which are effectively background independent, could be obtained for both deuterides and hydrides, with the well-documented differences between the cell volumes of the hydrides and deuterides being readily observed (Figure 32); the refined unit cell volume of both the Sr and Ba hydride is consistently larger than that of the corresponding deuteride over the entire temperature range. This difference in the cell volumes is commonly observed with saline hydrides and deuterides and is a result of the fundamental relationship between the phonon vibrational frequency and the isotope mass [105]. The extracted ADP's are self-consistent and generally show the expected trends as a function of temperature.

Figure 32 – The evolution of cell volume with temperature for SrH_2 (white triangles) and SrD_2 (black circles).

5.3 Hydrates

The structure of the newly synthesized compound $Cs(C_2O_4).H_2O$ (space group *C*2/*c*, unit cell volume ~750 $Å^3$), was initially determined by SCXD [39] and the hydrogen atoms located accurately and precisely by a 10 minute data collection on D20, an impressively short exposure time offering real potential for making such determinations routine and very easily accessible. The refinement was carried out using the joint SCXD-NPD approach described above, with the sensitivity of the neutron diffraction offering more chemically reasonable (and precise) values for the extracted O−H distance and the O−H−O internal angle in the H_2O molecule (0.964(7) Å and 111(1.0)°, respectively); these can be compared to the inaccurate determinations of 0.78(3) Å and 97(5)° from the SCXD data alone. The final joint refined structure is thus of very good quality as is the NPD profile fit (Figure 33).

As a further example of the power of NPD in the study of structural evolution in inorganic hydride and hydrate materials, and complementing the work presented above on molecular hydrates, the hydration behaviour of $CaSO_4$ under conditions of controlled humidity was undertaken, in a comprehensive study on D20. To reiterate, the ability to monitor changes in materials under controlled humidity *in-situ* is of potentially huge value to industry, materials and structural scientists, while from an experimental perspective, the possibility of studying hydration reactions *in situ,* through control of the relative humidity level, allows direct access to the structures of intermediate phases. Comparison of transformation behaviours and rates under different relative humidity levels also allows information to be extracted on the kinetics of the associated phase transformations.

Figure 33 – structure of $Cs(C_2O_4).H_2O$ (left) determined from joint SCXD-NPD refinement, with the final NPD fit shown (right).

$CuSO_4$ was chosen for this *in situ* study as an example of a system that undergoes hydrations as a series of distinct steps. Thermal dehydration of $CuSO_4.5H_2O$ shows stepwise decomposition *via* the trihydrate (formed at ~80°C), the monohydrate (formed above ~120°C) to (above ~240°C) anhydrous $CuSO_4$. Previous determinations of the water positions in the three hydrated phases of $CuSO_4$ had not adequately determined the hydrogen positions, an obvious area on which the NPD approach will have advantages. A powdered sample of $CuSO_4.5H_2O$ was dried to $CuSO_4$ at 400°C prior to exposure to 100% RH over 24 hrs, from which the NPD patterns showed the compound being converted from the pure anhydrous phase to the pure monohydrate (~5 hrs), then progressing to the trihydrate and the pentahydrate phases; the final patterns showed traces of all three hydrated phases. The structures of the intermediate phases (the mono and tri hydrate) were obtained by refinement using summed data sets (comprised of approximately 12 short data sets and roughly equivalent to 30 min data collections) which were taken over a period where the phase of interest was the majority phase. Using these structural descriptions of the intermediate phases, it was possible to use the short data sets to refine the phase fraction of each of the intermediate phases.

Figure 34 – the refined phase fractions of the anhydrous and hydrated phases of $CuSO_4$ as a function of exposure time at 100% RH, from the rapid scanning NPD data.

Figure 34 shows the evolution of the different hydrated phases, and the rate of transformation between them; for example, the rate of formation of the trihydrate is clearly slower than that of the monohydrate (consistent with the diffusion-controlled absorption of twice as many water molecules per mole). In addition to providing a powerful demonstration of the potential of this technique for such an *in situ* phase evolution study on hydrogenous systems, it is of interest that the expectation that $CuSO_4$ would convert completely to its monohydrate, trihydrate and pentahydrate in turn was not realised. Before the monohydrate had been completely converted to the trihydrate, the pentahydrate had already started to form.

6. Conclusions and Forward Look

This review has sought to indicate, by reference to a wide selection of our own studies, the initial establishment of the scope of neutron powder diffraction in the study of hydrogenous materials, an area

long regarded as difficult if not impossible to access. We have shown, in a wide range of materials, that when care is taken over experiment design and data collection, a wide range of systems can be studied, in both the molecular and materials domains. While impressive positive results are obtained in most of the cases studied during this programme, we have sounded a note of caution in a few areas, largely in molecular systems, in cases where complex, flexible or multiple molecule systems are being studied, or where NPD is being used in attempts to image proton disorder. Overwhelmingly, however, the success of this programme has opened a wide range of materials to study by this technique, and we have shown how advances in instrumentation have been a critical component of this, with the availability of next generation large detector arrays, high flux / high count-rate neutron powder diffractometers being key to this, together with advances in complementary sample handling and sample environment capabilities. Establishing these advanced instrument facilities makes this an area with exciting potential for exploitation both now and in the future, across a wide range of materials types, removing in most cases the need to deuterate samples prior to study by NPD.

We have thus demonstrated that neutron powder diffraction from high-flux sources under optimised conditions can be a valuable tool for the routine study of hydrogenous materials without having to resort to sample deuteration. The range of materials for which useful information can be extracted is extensive and covers many branches of inorganic, organometallic and organic chemistry. The limitations to the technique are usually related to the presence of crystallographically complex materials in which peak overlap in the powder diffraction pattern can be severe, or where the very highest *d*-spacing resolution might not be available for imaging of disordered protons. Without adequate resolution, the structural information on hydrogen embedded in the profile peak intensities of NPD data cannot be readily accessed or requires additional information (such as an SCXD data set or rigid body constraints) for it to be determined. Further developments in neutron diffraction instrumentation (particularly constant-wavelength instruments) are likely to lead to even more advances in this area, especially in terms of the crystallographic complexity of materials that can be studied. Improvements in both resolution and flux on the sample will also enable smaller samples to be studied. For example some of our recent results include structure solution and refinement of NPD data of rare hydrogenous minerals only available in 100 mg quantities. The hydrogen content of the material does not seem to be a factor in limiting this type of work though obviously the higher the hydrogen content the greater the experimental times required to achieve adequate peak-to-noise ratios. Even so, our preliminary studies have shown that hydrogen positions can be extracted from the analysis of NPD data sets collected from complex highly hydrogenous materials particularly when used in combination with SCXD data or with soft and/or rigid constraints.

The potential of the method discussed here is enormous given the extensive range of hydrogen-containing compounds and their importance in materials chemistry, geochemistry, life sciences and as energy materials. The ability to determine hydrogen positions in these compounds accurately, in a routine manner and from readily available material should impact enormously on our understanding of these areas of chemistry.

Acknowledgements

We would like to thank a range of colleagues who have contributed to this programme, including instrument scientists at ILL and ISIS – Thomas Hansen, Emmanuelle Suard, Richard Ibberson, Ron Smith – a range of academic collaborators for discussions, identification of potential areas of study and synthesizing compounds for study, including Andreas Danopoulos and Holger Kohlmann, and those undergraduate and graduate students who have contributed by preparing samples that have been utilized within this development programme. Parts of this work were funded under EPSRC awards EP/E050859, EP/E051049 and EP/I033459. Additional funding and support from STFC and ILL is acknowledged; beamtime and technical support at the neutron facilities have been invaluable in allowing much of this work to be carried out.

Notes on Contributors

Professor Chick Wilson, Chair of Physical Chemistry at the University of Bath, UK, was previously Visiting Professor in Durham and Tennessee, Regius Chair in Chemistry, University of Glasgow, Group Leader for Crystallography at the ISIS Neutron Source, and President of the British Crystallographic Association. His research interests include: hydrogen bonding; co-crystallisation as a route to new materials; crystallisation science, including flow crystallisation and self-assembly synthesis; crystal engineering of the organic solid state including polymorphism; dyes and optically-active materials; disorder in molecular materials; metastable state materials, and uses of neutron and synchrotron diffraction in chemistry.

Prof. Paul Henry received his BA in Chemistry (1993) and D. Phil. (1997) from the University of Oxford. After a PDRF at Southampton University, UK (1997-2003) he became instrument scientist for D20 at ILL, France (2003-2008), followed by instrument scientist for E9 at the BER-II reactor at the Helmholtz Zentrum Berlin, Germany (2008-2011). In 2011 he joined the European Spallation Source (ESS) as instrument scientist for diffraction to coordinate the design of the powder diffraction instrument suite for ESS. In May 2013 he became Adjunct Professor in Neutron Scattering at Chalmers University of Technology, Gothenburg, Sweden. His research interests lie in the fields of crystallography and instrumentation.

Dr Marc Schmidtmann is currently staff crystallographer at the University of Oldenburg, Germany. Previously he carried out post-doctoral research in materials chemistry at the University of Liverpool and in the study of hydrogenous molecular systems at the University of Glasgow. Previously, his PhD in structural chemistry from Glasgow followed a period as crystallographer in POM chemistry at the University of Bielefeld.

Dr Valeska Ting was appointed as the University of Bath's Prize Research Fellow in Smart Nanomaterials in 2012. Her research interests lie in the area of sustainable technologies. She is currently exploring the design of new nanomaterials for applications in hydrogen storage, carbon dioxide capture and in catalysis. She is also interested in the development of in-situ neutron scattering techniques for uncovering new information on the behaviour of hydrogen contained in nanoporous hydrogen storage materials.

Edward Williams was born in Aberystwyth, UK in 1987. He completed his MChem in Chemistry with Mathematics in 2009 at the University of Southampton. He went on to study for a PhD, again at the University of Southampton 2009-2013, investigating the behaviour of hydrogen within naturally occurring minerals, and the production of novel transition metal phosphate materials. Interests include inorganic chemistry, materials chemistry and crystallography of natural minerals.

Prof. Mark Weller is currently Professor of Energy Materials at the University of Bath, UK. His research interests cover a wide range of synthetic and structural materials chemistry in areas such as zeolites, rechargeable battery materials, specialist pigments and materials for harvesting sunlight. He also has an active interest in structural mineralogy and the potential of developing sustainable functional materials from naturally occurring minerals.

Subject Index

References

[1] Weller, M.T.; Henry, P.F.; Ting, V.P.; Wilson, C.C. Crystallography of hydrogen-containing compounds: realising the potential of neutron powder diffraction. *Chem. Commun.* **2009**, 2973-2989

[2] Onoda-Yamamuro, N.; Yamamuro, O.; Matsuo, T.; Ichikawa, M.; Ibberson, R.M.; David, W.I.F. Neutron diffraction study on hydrogen bond structure in $K_3H(SeO_4)_2$ and $K_3D(SeO_4)_2$ crystals. *J. Phys.: Condens. Matter* **2000**, *12*, 8559-8565.

[3] Krebs, F.C.; Jørgensen, M.; Lebech, B.; Frydenvang, K. A perdeuterated cryoprotectant for neutron studies and a demonstration of its use for neutron powder diffraction on L-(-)-ephedrine hemihydrate. *J. Appl. Cryst.* **2001**, *34*, 203-207.

[4] Suzuki, A.; Ohtani, E.; Kondo, T.; Kuribayash, T. Neutron diffraction study of hydrous phase G: Hydrogen in the lower mantle hydrous silicate, phase G. *Geophys. Res. Letts.* **2001**, *28*, 3987-3990.

[5] Hoshikawa, A.; Igawa, N.; Yamauchi, H.; Ishii Y. Neutron powder diffraction study of methane deuterohydrate by the maximum entropy method. *J. Phys. Chem. Solids* **2005**, *66*, 1810-1814.

[6] Dincă, M.; Dailly, A.; Liu, Y.; Brown, C.M.; Neumann, D.A.; Long J.R. Hydrogen storage in a microporous metal-organic framework with exposed Mn2+ coordination sites. *J. Am. Chem. Soc.* **2006**, *128*, 16876-16883.

[7] Hoepfner, V.; Jacobs, P.; Sawinski, P.K.; Houbnen, A.; Reim, J.; Dronskowski, R. $RbCN_3H_4$ and $CsCN_3H_4$: A Neutron Powder and Single Crystal X-ray Diffraction Study. *Z. Anorg. Allg. Chem.* **2013**, *639*, 1232-1236.

[8] Xia, F.; O'Neill, B.; Ngothai, Y.; Peak, J.; Tenailleau, C.; Etschmann, B.; Qian, G.; Brugger, J.; Studer, A.; Olsen, S.; Pring, A. A thermosyphon-driven hydrothermal flow-through cell for in situ and time-resolved neutron diffraction studies. *J. Appl. Cryst.* **2010**, *43*, 511-519.

[9] Verdal, N.; Udovic, T.J.; Rush, J.J.; Wu, H.; Skripov, A.V. Evolution of the Reorientational Motions of the Tetrahydroborate Anions in Hexagonal $LiBH_4$–LiI Solid Solution by High-Q Quasielastic Neutron Scattering. *J. Phys. Chem. C* **2013**, *117*, 12010-12018.

[10] Wilson, C.C. 2000, *Single Crystal Neutron Diffraction from Molecular Materials*, World Scientific, Singapore, ISBN-981-02-3776-6.

[11] Wilson, C.C. The evolution of hydrogen atom parameters under changing external conditions by time-of-flight single crystal neutron diffraction. *Cryst. Revs.*, 2007, **13**, 143-198.

[12] Wilson. C.C. A basic introduction to thermal motions of atoms in crystal structures, the underlying potentials and the physical information available from their analysis. *Cryst. Revs.* **2009**, *15*, 3-56.

[13] Allen, F.H.; Howard, J.A.K.; Hoy, V.J.; Desiraju, G.R.; Reddy, D.S.; Wilson, C.C. First neutron diffraction analysis of an O-H...π hydrogen bond: 2-ethynyl-2-adamantanol. *J. Amer. Chem. Soc.* **1996**, *118*, 4081-4084.

[14] Bilton, C.; Howard, J.A.K.; Madhavi, N.N.L.; Nangia, A.; Desiraju, G.R.; Allen, F.H.; Wilson, C.C. When is a polymorph not a polymorph? Helical trimeric O-H…O synthons in *trans*-1,4,-diethynyl-1,4-cyclohexanediol. *Chem. Commun.* **1999**, 1675-1676.

[15] Coppens, P.; Vos, A. Electron density distribution in cyanuric acid. II. Neutron diffraction study at liquid nitrogen temperature and comparison of X-ray neutron diffraction results. *Acta Crystallogr. Sect. B.* **1971**, *27*, 146-158.

[16] Schmidtmann, M.; Farrugia, L.J.; Middlemiss, D.S.; Gutmann, M.J.; McIntyre, G. J.; and Wilson, C.C. Experimental and Theoretical Charge Density Study of the Polymorphic Molecular Complexes of Isonicotinamide with Oxalic Acid. *J. Phys. Chem. B* **2009**, *113*, 13985-13997

[17] Wilson, C.C. Beyond the thermal ellipsoid in molecular crystal structures. *Recent Res. Devel. Chem. Phys.* **2002**, *3*, 119-147.

[18] Wilson, C.C.; Thomas, L.H. The short hydrogen bond in molecular materials: neutron diffraction and complementary studies. *Comptes Rendus* **2005**, *8*, 1434-1443.

[19] Wilson, C.C.; Shankland, N.; Florence, A.J. Direct determination of the temperature dependence of proton transfer in the benzoic acid dimer by single crystal neutron diffraction. *Chem. Phys. Lett.* ***1996***, 253, 103-107.

[20] Wilson, C.C. Migration of the proton in the strong hydrogen bond in urea-phosphoric acid. *Acta Crystallogr. Sect. B* **2001**, *57*, 435-439.

[21] Wilson, C.C.; Shankland, K.; Shankland, N. Single-crystal neutron diffraction of urea-phosphoric acid: evidence for H-atom migration in a short hydrogen bond between 150K and 350K. *Z. Kristallogr.* **2001**, *216*, 303-306.

[22] Steiner, T.; Majerz, I.; Wilson, C.C. First O-H-N Hydrogen Bond with a Centered Proton Obtained by Thermally Induced Proton Migration. *Angew. Chem. Int. Ed. Engl.*, **2001**, *40*, 2651-2654.

[23] Cowan, J.A.; Howard, J.A.K.; McIntyre, G.J.; Lo, S.M.-F.; Williams, I.D. Variable-temperature neutron diffraction studies of the short, strong N...O hydrogen bonds in the 1:2 co-crystal of benzene-1,2,4,5-tetracarboxylic acid and 4,4'-bipyridyl. *Acta Crystallogr. Sect. B* **2003**, *59*, 794-801.

[24] Cowan, J.A.; Howard, J.A.K.; McIntyre, G.J.; Lo, S.M.-F.; Williams, I.D. Variable-temperature neutron diffraction studies of the short, strong hydrogen bonds in the crystal structure of pyridine-3,5-dicarboxylic acid. *Acta Crystallogr. Sect. B* **2005**, *61*, 724-730.

[25] Wilson, C.C. Interesting proton behaviour in molecular structures. Variable temperature neutron diffraction and *ab initio* study of acetylsalicylic acid: characterising librational motions and comparing protons in different hydrogen bonding potentials. *New J. Chem.* **2002**, *26*, 1733-1739.

[26] Jones, A.O.F.; Blagden, N.; McIntyre, G.J.; Parkin, A.; Seaton, C.C.; Thomas, L.H.; Wilson, C.C. Tuning Proton Disorder in 3,5-Dinitrobenzoic Acid Dimers: the Effect of Local Environment. *Cryst. Growth Des.* **2013**, *13*, 497-509.

[27] Destro, R. Proton transfer in the solid state: therymodynamic parameters from an X-ray study in the temperature range 20–293K. *Chem. Phys. Letts.* **1991**, *181*, 232-236.

[28] Wilson, C.C.; Goeta, A.E. Direct imaging of proton disorder in a hydrogen-bonded carboxylic acid dimer by variable temperature X-ray diffraction. *Angew. Chem. Int. Ed. Engl.* **2004**, *43*, 2095-2099.

[29] Nygren, C.L.; Wilson, C.C.; Turner, J.F.C. On the solid state structure of 4-iodobenzoic acid. *J. Phys. Chem. A* **2005**, *109*, 2586-2593.

[30] Vyas, M.; Sakore, T. D.; Biswas, A.B. The structure of p-dimethylaminobenzoic acid. *Acta Crystallogr. Sect. B* **1978**, *34*, 1366-1368.

[31] Anulewicz, R.; Haefelinger, G.; Krygowski, T.M.; Regelmann, C.; Ritter, G. *Z. Naturforsch. B, Chem. Sci.* **1987**, *42*, 917.

[32] Sharma, C.V.K.; Panneerselvam, K.; Pilati, T.; Desiraju, G. R. Molecular recognition involving an interplay of O–H...O, C–H...O and π...π interactions. The anomalous crystal structure of the 1 : 1 complex 3,5-dinitrobenzoic acid–4-(N,N-dimethylamino)benzoic acid. *J. Chem. Soc., Perkin Trans. 2* **1993**, 2209-2216.

[33] Parkin, A.; Harte, S.M.; Goeta, A.E.; Wilson, C.C. Imaging proton migration from X-rays and neutrons. *New J. Chem.* **2004**, *28*, 718-721.

[34] Wilson, C.C.; Thomas. L.H.; Morrison, C.A. A symmetric hydrogen bond revisited: potassium hydrogen maleate by variable temperature, variable pressure neutron diffraction and plane-wave DFT methods. *Chem. Phys. Lett.* **2003**, *381*, 102-108.

[35] Morrison, C.A.; Siddick, M.M.; Camp, P.J.; Wilson, C.C. Towards understanding mobile proton behaviour from first principles: the short hydrogen bond in urea-phosphoric acid. *J. Amer. Chem. Soc.* **2005**, *127*, 4042-4048.

[36] Bernal, I.; Korp, J.D.; Schlemper, E.O.; Hussain, M.S. The crystal and molecular structures of $[Co(NH_3)_6][CuCl_5]$ as determined from single crystal X-ray and neutron diffraction data. *Polyhedron* **1982**, *1*, 365-369.

[37] Bau, R.; Drabnis, M.H.; Garlaschelli, L.; Klooster, W.T.; Xiem, Z.W.; Koetzle, T.F.; Martinengo, S. Five-Coordinate Hydrogen: Neutron Diffraction Analysis of the Hydrido Cluster Complex $[H_2Rh_{13}(CO)_{24}]^{3-}$. *Science* **1997**, *275*, 1099-1102.

[38] Leech, C.K.; Fabbiani, F.P.A.; Shankland, K.; David, W.I.F.; Ibberson, R.M. Accurate molecular structures of chlorothiazide and hydrochlorothiazide by joint refinement against powder neutron and X-ray diffraction data. *Acta Crystallogr. Sect. B* **2008**, 64, 101-107

[39] Weller, M.T.; Henry, P.F.; Light, M.E. Rapid structure determination of the hydrogen-containing compound Cs2C2O4·H2O by joint single-crystal X-ray and powder neutron diffraction. *Acta Crystallogr. Sect. B* **2007**, *63*, 426-432.

[40] Chater, P.A.; David, W.I.F.; Johnson, S.R.; Edwards, P.P.; Anderson, P.A. Synthesis and crystal structure of $Li_4BH_4(NH_2)_3$. *Chem. Commun.* **2006**, 2439-2441.

[41] Bostrom, M.; Gemmi, M.; Schnelle, W.; Eriksson, L. Synthesis, properties and structure determination of $Nb_2O_3(SO_4)_2{\cdot}14H_2O$ from neutron and synchrotron X-ray powder diffraction data. *J. Solid State Chem.* **2004**, *177*, 1738-1745.

[42] Campbell, B.J.; Cheetham, A.K.; Vogt, T.; Carluccio, L.; Parker, W.O.; Flego, C.; Millini, R. The Determination of Brønsted Acid Sites in Zeolite ERS-7 by Neutron and X-ray Powder Diffraction. *J. Phys. Chem. B* **2001**, *105*, 1947-1955.

[43] Morris, R.E.; Harrison, W.T.A.; Nicol, J M.; Wilkinson, A.P.; Cheetham, A.K. Determination of complex structures by combined neutron and synchrotron X-ray powder diffraction. *Nature* **1992**, *359*, 519-522.

[44] http://www.ill.eu/

[45] Böni, P. Supermirror Based Beam Devices. *Physica B* **1997**, *234-236*, 1038.

[46] http://neutrons.ornl.gov/facilities/facilities_hfir.shtml

[47] http://www.isis.rl.ac.uk/

[48] http://www.frm2.tu-muenchen.de/

[49] http://www.ansto.com.au/opal/

[50] http://neutrons.ornl.gov/facilities/facilities_sns.shtml

[51] http://j-parc.jp/ (http://j-parc.jp/index-e.html)

[52] http://europeanspallationsource.se/

[53] David, W.I.F.; Shankland, K.; McCusker, L.B.; Baerlocher, C. *Structure Determination from Powder Diffraction Data*, Oxford Univ. Press, Oxford, **2002**.

[54] Hewat, A.W. High flux diffractometers on reactor neutron sources. *Physica B* **2006**, *385-386*, 979-984.

[55] Studer, A.J.; Hagen, M.E.; Noakes, T.J. Wombat: The high-intensity powder diffractometer at the OPAL reactor. *Physica B* **2006**, *385-386*, 1013-1015.

[56] Day, P.; Enderby, J.E.; Williams, W.G.; Chapon, L.C.; Hannon, A.C.; Radaelli, P.G.; Soper, A.K. GEM: The General Materials Diffractometer at ISIS – Multibank Capabilities for Studying Crystalline and Disordered Materials. *Neutron News* **2004**, *15*, 19

[57] Huq, A.; Hodges, J.P.; Gourdon, O.; Heroux, L. POWGEN: a third-generation high resolution high-throughput powder diffraction instrument at the Spallation Neutron Source. *Z. Kristallogr. Proceedings* **2011**, *1*, 127-135.

[58] Arima, H.;T. Hattori, T.;Komatsu, K.; Abe, J.;Utsumi, W.;Kagi, H.; Suzuki, A.; Suzuya, K.;Kamiyama, T.; Arai, M.;Yagi, T.. Designing PLANET: Neutron beamline for high-pressure material science at J-PARC. *J Phys: Conf. Series* **2010**, *215*, 012025.

[59] Henry, P.F.; Weller, M.T.; Wilson, C.C. Neutron powder diffraction in materials with incoherent scattering: An illustration of Rietveld refinement quality from non-deuterated gypsum. *J. Appl. Cryst.* **2009**, *42*, 1176-1188.

[60] Kuhs, W.F. Unpublished work, *ILL experiment number 5-25-150*, **2008**

[61] Schmitt, D.; Ouladdiaf, B. Absorption Correction for Annular Cylindrical Samples in Powder Neutron Diffraction. *J. Appl. Crystallogr.* **1998**, *31*, 620-624.

[62] Mercury, J.M.R.; Pena, P.; de Aza, A.H.; Sheptyakov, D.; Turrillas, X. On the Decomposition of Synthetic Gibbsite Studied by Neutron Thermodiffractometry. *J. Amer. Ceram. Soc.* **2006**, *89*, 3728-3733.

[63] Larson, A.C.; von Dreele, R B. GSAS: General Structure Analysis System. *Los Alamos National Laboratory Report*, **1994**, 86-748

[64] Caira, M.R.; Bettinetti, G.; Sorrenti, M. Structural relationships, thermal properties, and physicochemical characterization of anhydrous and solvated crystalline forms of tetroxoprim. *J. Pharm. Sci.* **2002**, *91*, 467-481

[65] David, W.I.F.; Shankland, K. Structure determination from powder diffraction data. *Acta Crystallogr. Sect. A* **2008**, *64*, 52-64.

[66] Tremayne, M. The impact of powder diffraction on the structural characterization of organic crystalline materials. *Phil. Trans. Roy. Soc. London, Series A* **2004**, *362*, 2691-2707.

[67] Shankland, K.; David, W.I.F.; Sivia, D.S. Routine ab initio structure determination of chlorothiazide by X-ray powder diffraction using optimised data collection and analysis strategies. *J. Mater. Chem.* **1997**, *7*, 569-572.

[68] Martins, D.M.S.; Middlemiss, D.S.; Pulham, C.R.; Wilson, C.C.; Weller, M.T.; Henry, P.F.; Shankland, N.; Shankland, K.; Marshall, W.G.; Ibberson, R.M.; Moggach, S.; Brunelli, M.; Morrison, C.A. Temperature-induced Proton Transfer in the 1:1 Adduct formed between Squaric Acid and 4,4'-Bipyridine. *J. Amer. Chem. Soc.* **2009**, *131*, 3884-3893.

[69] Schmidtmann, M.; Gutmann, M.J.; Middlemiss, D.S.; Wilson, C.C. Towards Proton Transfer in Hydrogen Bonded Molecular Complexes: Joint Experimental and Theoretical Modelling and an Energy Scale for Polymorphism. *CrystEngComm* **2007**, *9*, 743-745.

[70] Schmidtmann, M.; Coster, P.; Henry, P.F.; Ting, V.P.; Weller, M.T.; Wilson, C.C. Determining hydrogen positions in crystal engineered organic molecular complexes by joint neutron powder and single crystal X-ray diffraction. *CrystEngComm*, **2014**, DOI: 10.1039/C3CE42070A.

[71] Schmidtmann, M.; Wilson, C.C. Hydrogen transfer in pentachlorophenol – dimethylpyridine complexes. *CrystEngComm* **2008**, *10*, 177-183.

[72] Dittrich, B.; Spackman, M.A. Can the interaction density be measured? The example of the non-standard amino acid sarcosine. *Acta Crystallogr. Sect. A* **2007**, *63*, 426-436.

[73] Rowe, R.C.; Sheskey, P.J.; Owen, S.C. eds. *Handbook of Pharmaceutical Excipients*, Fifth edition, **2005**, Pharmaceutical Press London

[74] Jeffrey, G.A.; Nanni, R. The crystal structure of anhydrous α,α-trehalose at −150°. *Carbohydr. Res.* **1985**, *137*, 21-30.

[75] Harris, K.D.M. Modern applications of Powder X-ray diffraction in pharmaceutical sciences. *American Pharmaceutical Review* **2004**, *7*, 86–91

[76] MacCalman, M.L.; Roberts, K.J.; Kerr, C.; Hendriksen, B. On-line processing of pharmaceutical materials using in situ X-ray diffraction. *J. Appl. Crystallogr.* **1995**, *28*, 620

[77] Davis, T.D.; Morris, K.R.; Huang, H.; Peck, G.E.; Stowell, J.G.; Eisenhauer, B.J.; Hilden, J.L.; Gibson, D.; Byrn, S.R. In situ monitoring of wet granulation using online X-ray powder diffraction. *Pharm. Res.* **2003**, *20*, 1851-1857.

[78] Ting, V.P.; Schmidtmann, M.; Wilson, C.C.; Weller, M.T. Cisplatin - Polymorphism and New Structural Insights into an Important Chemotherapeutic Drug. *Angew. Chem.* **2010**, *49*, 9408–9411.

[79] Flechon, A.; Culine, S.; Droz, J.P. Intensive and timely chemotherapy, the key of success in testicular cancer. *Crit. Rev. Oncol. Hematol.* **2001**, *37*, 35-46.

[80] Prestayko, A.W.; Crooke, S.T.; Carter, S.K. *Cisplatin, current status and new developments*, New York : Academic Press **1980**.

[81] Milburn, G.H.W.; Truter, M.R. The crystal structures of cis- and trans-dichlorodiammineplatinum(II). *J. Chem. Soc. (A)* **1966**, 1609-1616.

[82] Wilson, C.C.; Xu, X.; Florence, A.J.; Shankland, N. Temperature dependence of proton transfer in 4-chlorobenzoic acid. *New J. Chem.* **2006**, *30*, 979-981.

[83] Leiserowitz, L. Molecular packing modes. Carboxylic acids. *Acta Crystallogr. Sect. B* **1976**, *32*, 775-802.

[84] Florencio, F.; Smith, P. The crystal structure of 2,4,6-trimethylbenzoic acid. *Acta Crystallogr. Sect. B* **1970**, *26*, 659-666.

[85] Benghia, V.; Leiserowitz, L. Molecular packing modes. Part IX. Crystal and molecular structures of pentafluorobenzoic acid and mesitoic acid. *J. Chem. Soc. Perkin Trans. II* **1972**, 1778-1785.

[86] Schofield, P.F.; Wilson, C.C.; Knight, K.S.; Stretton, I.C. Temperature related structural variation of the hydrous components in gypsum. *Z. Kristallogr.* **2000**, *215*, 707-710.

[87] Schofield, P.F.; Knight, K.S.; Stretton, I.C. Thermal expansion of gypsum investigated by neutron powder diffraction. *Amer. Mineral.* **1996**, *81*, 847-851.

[88] Galameau, A.; Di Renzo, F.; Fajula, F.; Vedrine, J. eds. *Zeolites and Mesoporous Materials at the Dawn of the 21st Century*, Elsevier, Amsterdam, **2001**.

[89] Aiello, R.; Giordano, G.; Testa F. eds. *Impact of Zeolites and Other Porous Materials on the New Technologies at the Beginning of the New Millennium,* Elsevier, Amsterdam, **2002**.

[90] Henry, P.F.; Weller, M.T.; Wilson, C.C. Hydrogenous materials using powder neutron diffraction: full structural determination of adsorbed water molecules in a zeolite. *Chem. Commun.* **2008**, 1557-1559.

[91] Ting, V.P.; Henry, P.F.; Schmidtmann, M.; Wilson, C.C.; Weller, M.T. In-situ neutron powder diffraction and structure determination in controlled humidities. *Chem. Commun.* **2009**, 7527-7529.

[92] Wilson, C.C. Structural studies of Schultenite in the temperature range 125K to 324K by pulsed single crystal neutron diffraction - hydrogen ordering and structural distortions. *Mineral. Mag.* **1994**, *58*, 629-634.

[93] Tun, Z.; Nelmes, R.J.; Kuhs, W.F.; Stansfield, R.F.D. A high-resolution neutron-diffraction study of the effects of deuteration on the crystal structure of KH_2PO_4. *J. Phys. C* **1988**, *21*, 245-258.

[94] Armstrong, J.A.; Friis, H.; Lieb, A.; Finch, A.A.; Weller, M.T. Combined single-crystal X-ray and neutron powder diffraction structure analysis exemplified through full structure determinations of framework and layer beryllate minerals. *Amer. Mineral.* **2010**, *95*, 519-526.

[95] Cannillo, E.; Coda, A.; Fagnani, G. The crystal structure of bavenite. *Acta Crystallogr.* **1966**, *20*, 301–309.

[96] Williams, E.R.; Weller, M.T. A variable-temperature neutron diffraction study of ussingite; a strong asymmetric hydrogen bond in an aluminosilicate framework. *Phys. Chem. Minerals* **2012**, *39*, 471-478.

[97] Jacobsen, S.D.; Smyth, J R.; Swope, R.J.; Sheldon, R.I. Two proton positions in the very strong hydrogen bond of serandite, $NaMn_2[Si_3O_8(OH)]$. *Amer. Mineral.* **2000**, *85*, 745-752.

[98] Laughon, R.B. The crystal structure of kinoite. *Amer. Mineral.* **1971**, *56*, 193-200.

[99] Piccoli, P.M.B.; Koetzle, T.F.; Schultz, A.J. Single crystal neutron diffraction for the inorganic chemist – a practical guide. *Comments on Inorganic Chemistry* **2007**, *28*, 3-38.

[100] Black, M.; Mais, R.H.B.; Owston, P.G. The crystal and molecular structure of Zeise's salt, $KPtCl_3.C_2H_4.H_2O$. *Acta Crystallogr. Sect. B* **1969**, *25*, 1753-1759.

[101] Jarvis, J.A.J.; Kilbourn, B.T.; Owston, P.G. Redetermination of crystal and molecular structure of Zeise's salt, $KPtCl_3.C_2H_4.H_2O$. *Acta Crystallogr. Sect. B* **1970**, *27*, 366-372.

[102] Love, R.A.; Koetzle, T.F.; Williams, G.J.B.; Andrews, L.C.; Bau, R. Neutron diffraction study of the structure of Zeise's salt, $KPtCl_3(C_2H_4).H_2O$. *Inorg. Chem.* **1975**, *14*, 2653-2657.

[103] Brese, N.E.; O'Keeffe, M.; von Dreele, R.B. Synthesis and crystal structure of SrD_2 and SrND and bond valence parameters for hydrides. *J. Solid State Chem.* **1990**, *88*, 571-576.

[104] Ting, V.P.; Henry, P.F.; Kohlmann, H.; Wilson C.C.; Weller, M.T. Structural isotope effects in metal hydrides and deuterides. *PhysChemChemPhys* **2010**, *12*, 2083-2088.

[105] Plekhanov, V.G. in *International Symposium on Isotope Science and Engineering from Basics to Applications* (ISE 2005), Atomic Energy Soc. Japan, Nagoya, JAPAN, 2005, pp. 375-381.

- 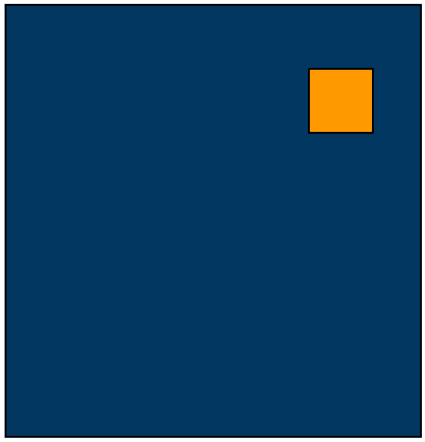

Figure 1 – Comparison of ^{1}H (H) and ^{2}H (D) incoherent scattering cross-sections, showing the reduction in this cross section for D (represented by the light area).

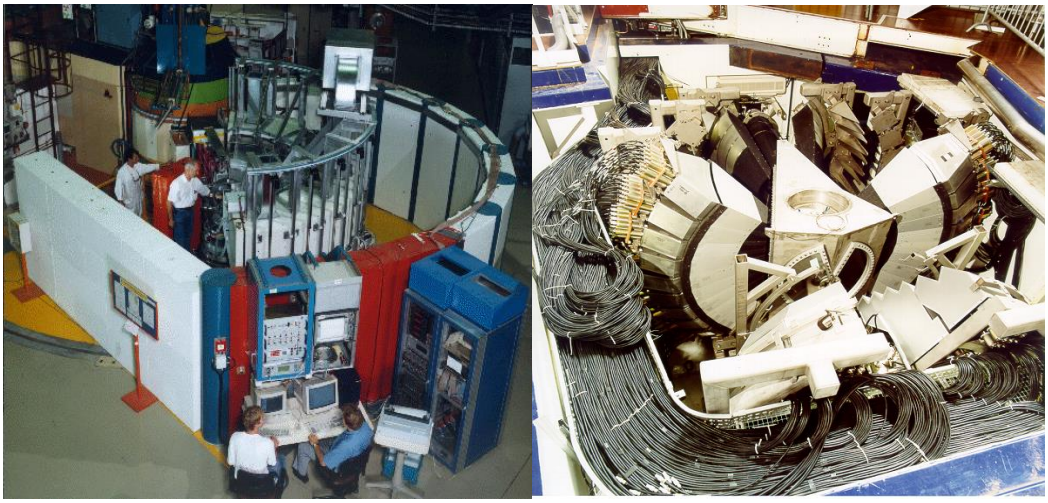

Figure 2 – the high flux neutron powder diffractometers D20 (left) and GEM (right)

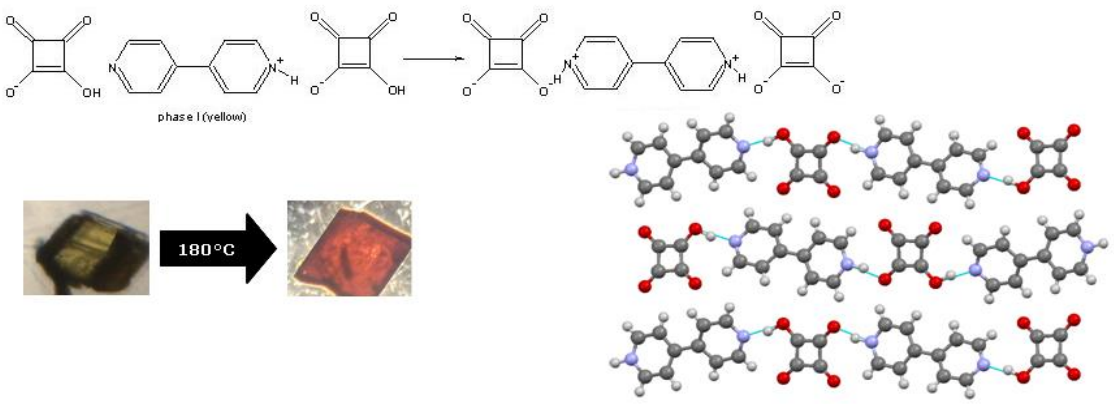

Figure 3 – the thermochromic phase transition in 1:1 squaric acid:4,4'-bipyridine is due to proton transfer and has been characterised by a range of techiques including NPD.

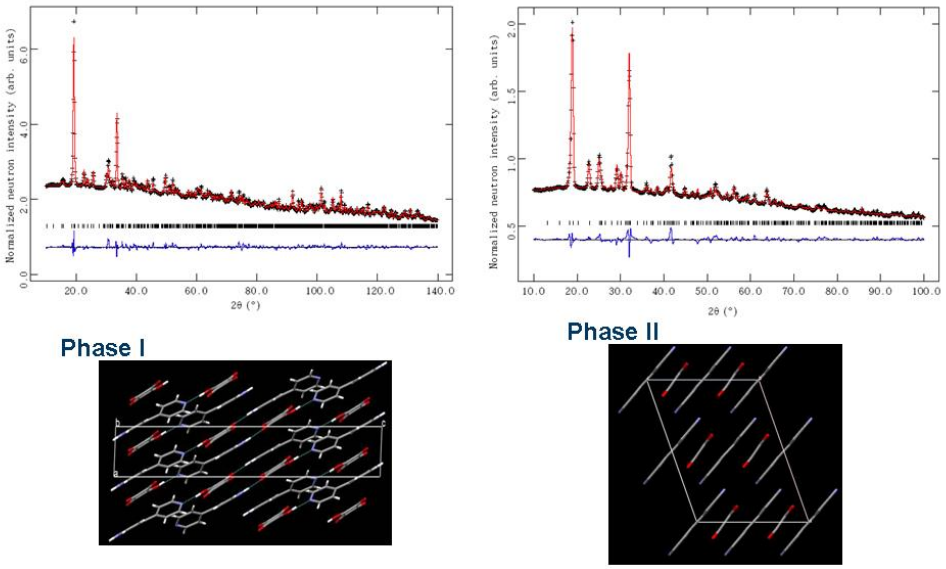

Figure 4 – high quality NPD data and good quality Rietveld fits were obtained for both polymorphs of 1:1 squaric acid:4,4'-bipyridine.

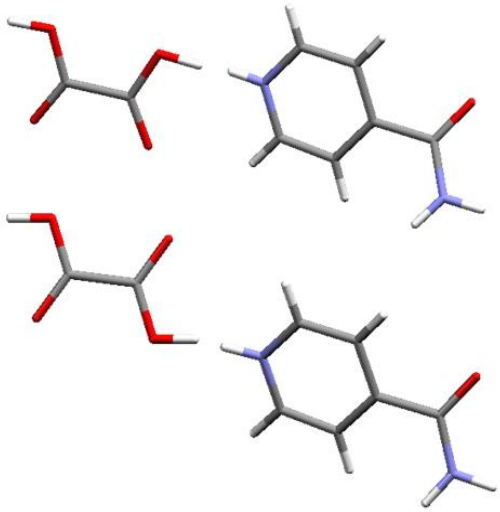

Figure 5 – The two polymorphs of IN_2-OA exhibit "cis" (Form I, top) and "trans" (Form II, bottom) conformation of the oxalic acid with respect to the isonicotinamide.

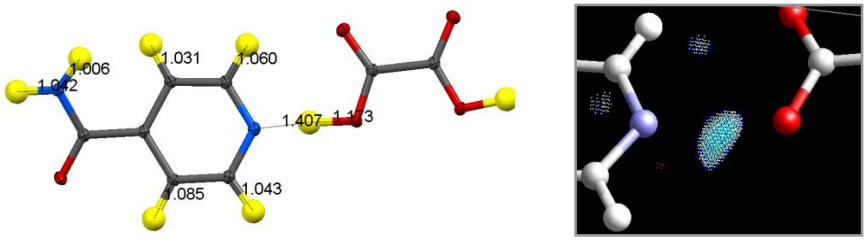

Figure 6 – Refined bond lengths to H atoms (left) and Fourier map in the region of the strong hydrogen bond (right), from the combined neutron-X-ray refinement of Form I of IN_2-OA.

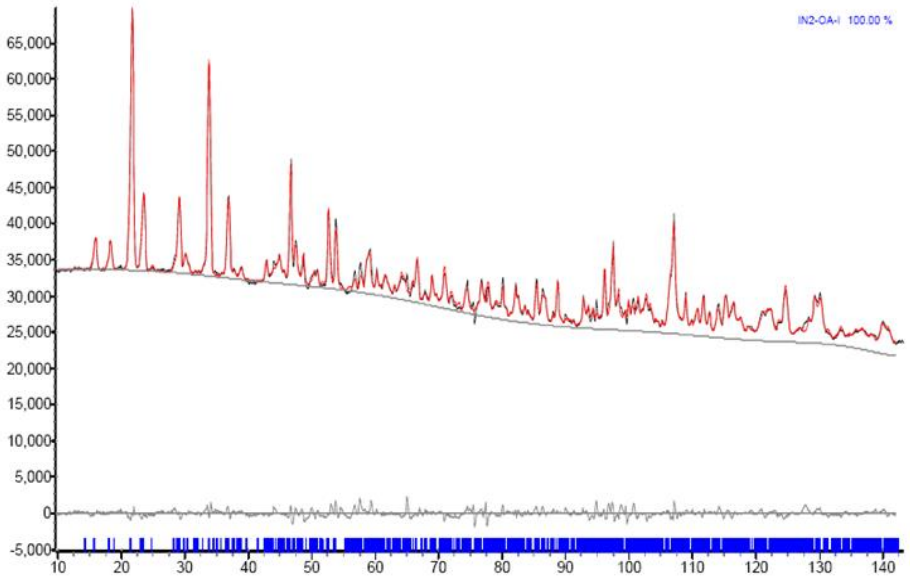

Figure 7 – Rietveld fit for the NPD data, with the model resulting from the combined refinement of Form I of IN_2-OA.

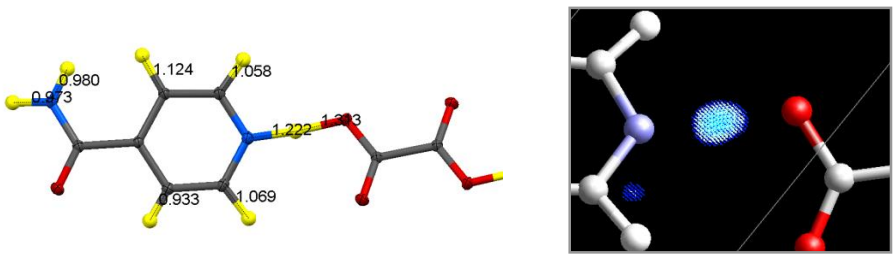

Figure 8 – Refined bond lengths to H atoms (left) and Fourier map in the region of the strong hydrogen bond (right), from the combined neutron-X-ray refinement of Form II of IN_2-OA.

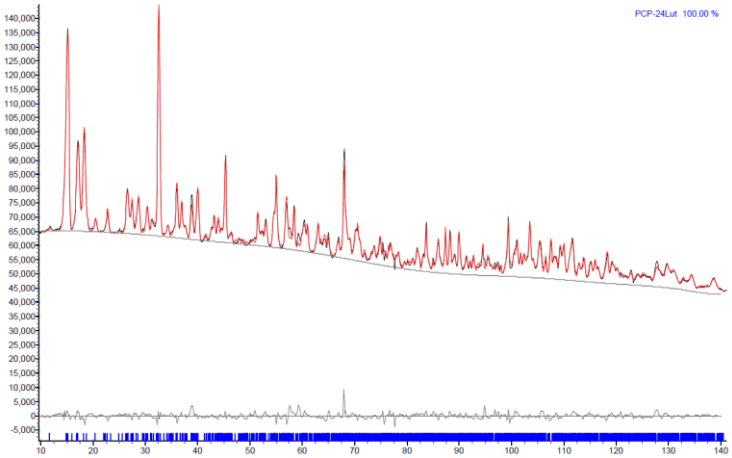

Figure 9 – Typical Rietveld fit from D20 study of PCP-lutidine complexes, specifically for the 2,4-lutidine complex.

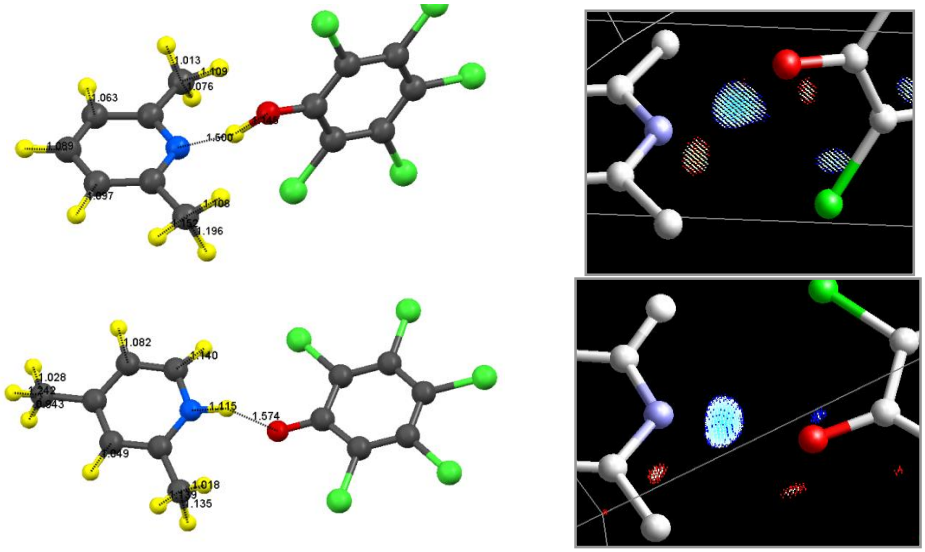

Figure 10 – Refined bond lengths to selected H atoms (left) and Fourier map in the region of the strong hydrogen bond (right), from the combined neutron-X-ray refinement of PCP:2,6-lutidine (top) and PCP:2,4-lutidine (bottom).

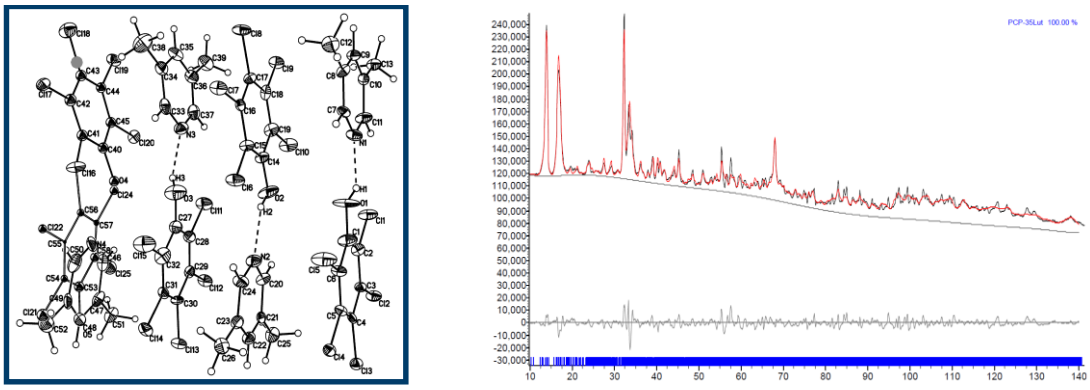

Figure 11 – The NPD study of the PCP:3,5-lutidine complex with a large asymmetric unit containing multiple molecules proved not to be able to yield an adequate structural refinement.

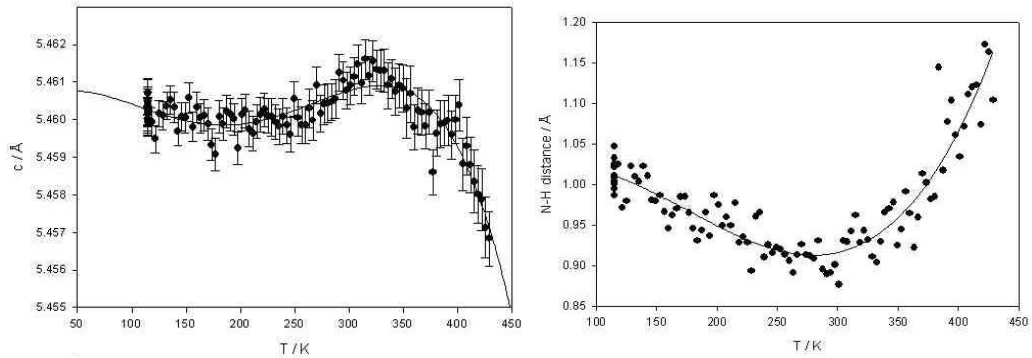

Figure 12 – Variable temperature neutron powder diffraction of glycine allows structural trends between molecular geometry (N-H1 distance, right) and unit cell parameters (c – left) to be correlated.

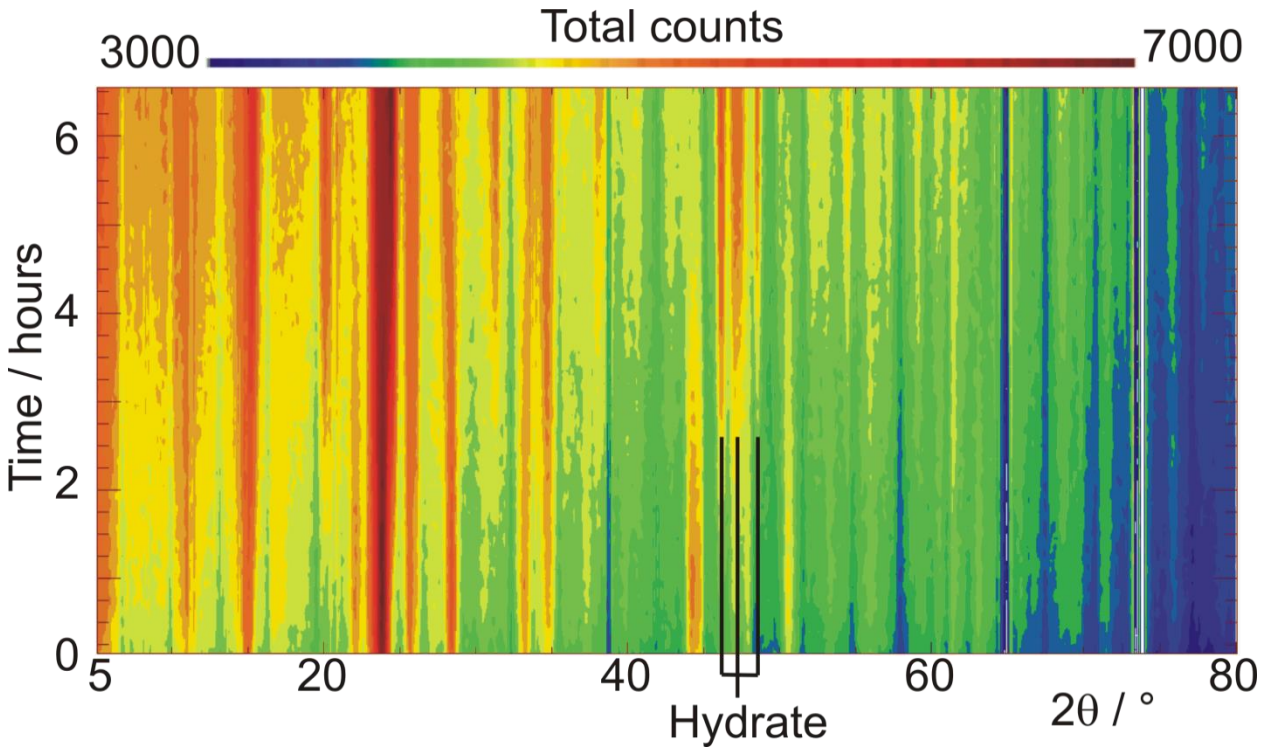

Figure 13 – Stacked plot viewed down the intensity direction showing the evolution of the diffraction patterns of standard stable α-lactose as a function of time in 100% relative humidity at 45°C; the positions of three strong reflections from α-lactose monohydrate are shown.

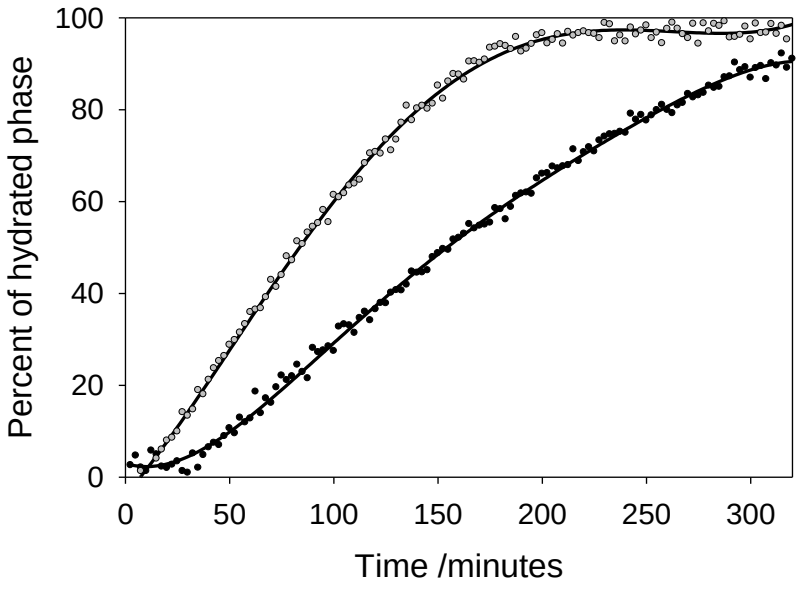

Figure 14 – Phase percentage of α-lactose monohydrate as a function of time in highly crystalline (black filled circles) and small particle size (grey filled circles) forms.

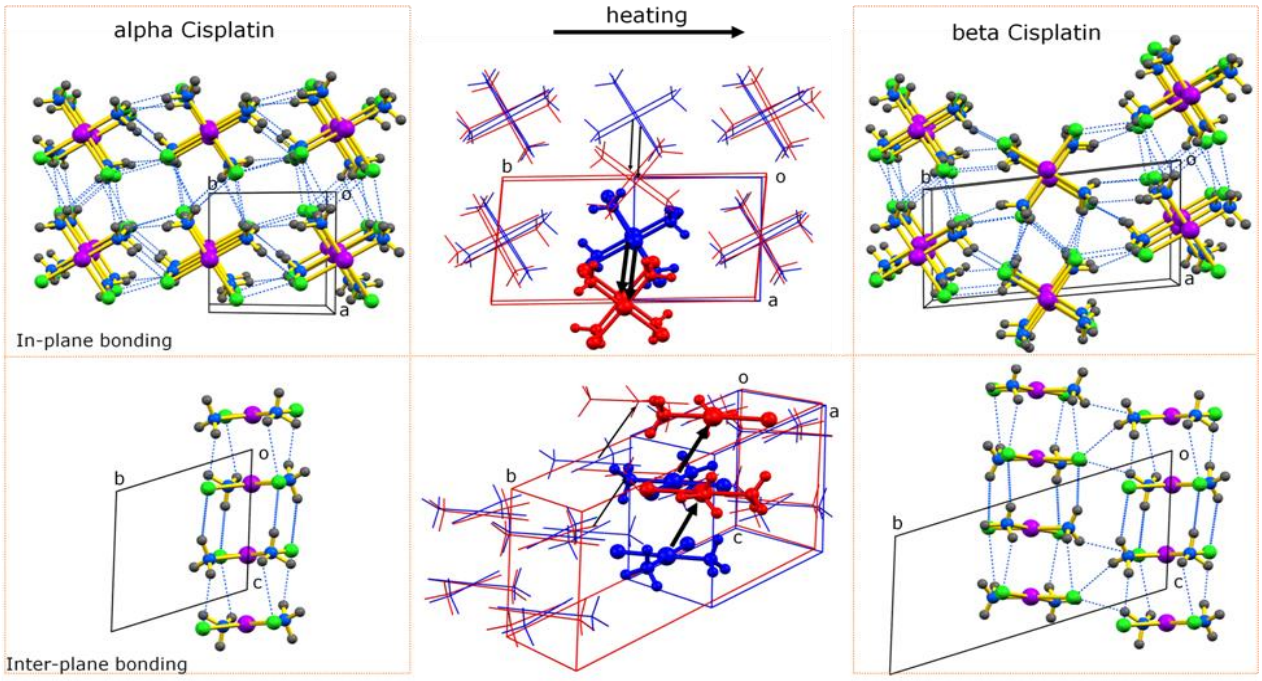

Figure 15 – the transformation between the crystalline forms of cisplatin: (left) the structure of the alpha form showing the layers of molecules in the ab plane (top) and highlighting the H-bonding (dashed blue lines) between the layers along c (bottom); (centre) the overlaid unit cells of the alpha and beta forms, showing the transformation under heating from the low T alpha form (blue) to the high T beta form (red); (right) the structure of the beta form, showing the layers in the ab plane (top) and showing the H-bonding between the layers along c (bottom).

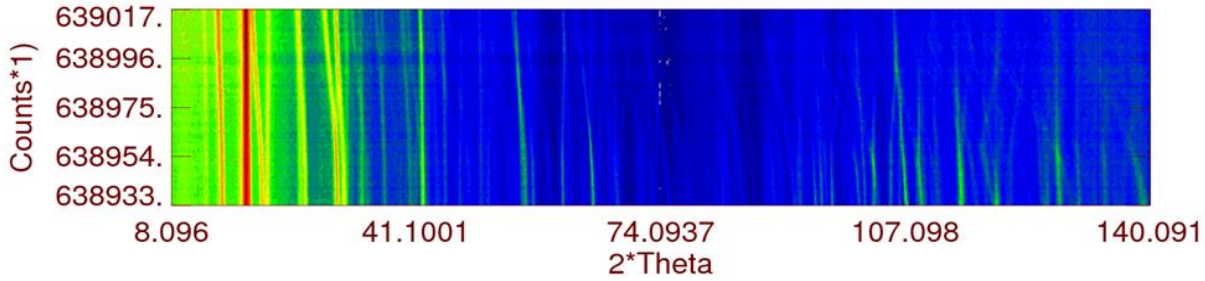

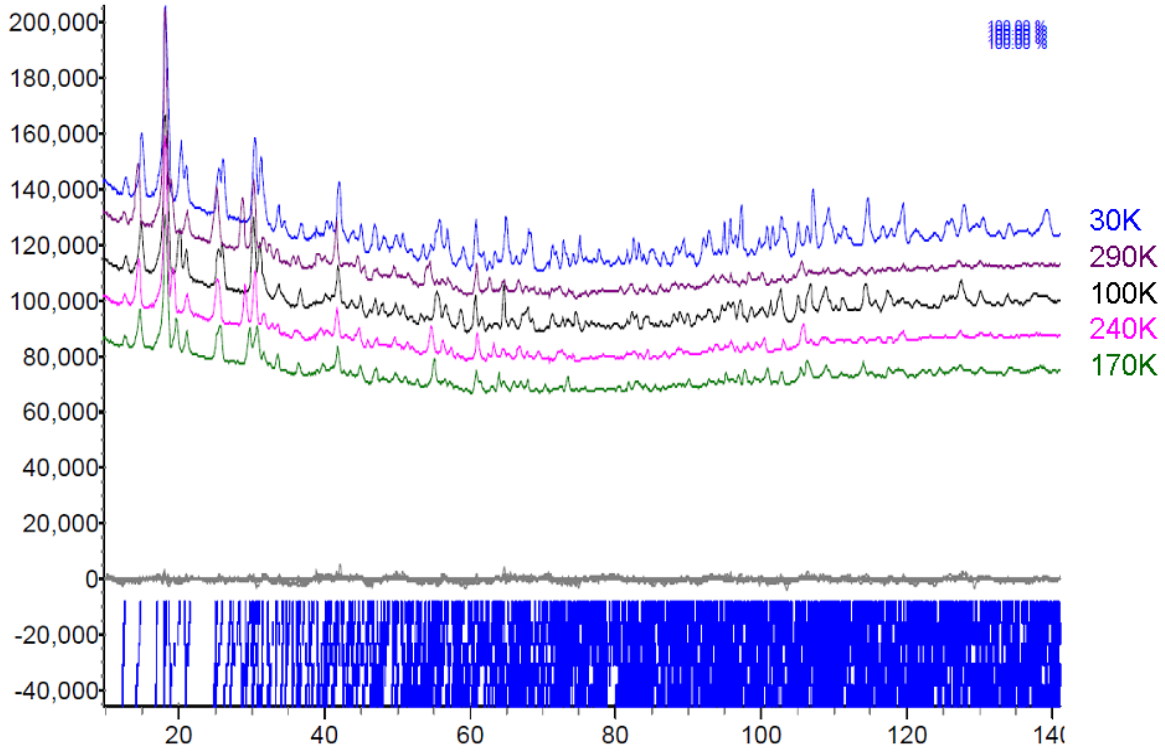

Figure 16 – NPD pattern evolution in the thermodiffractometry experiment (top) and individual diffraction patterns (bottom) from the D20 experiment on 2,4,6-trimethylbenzoic acid.

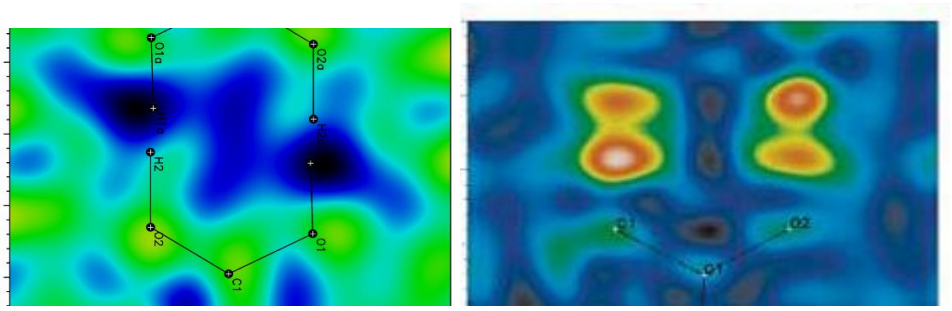

Figure 17 – Fourier maps in the region of the carboxylic acid dimer in 2,4,6-trimethylbenzoic acid with the hydrogen atoms removed. The inconclusive map from the NPD data (left) can be compared with the clear indication of disordered H atom density from the single crystal X-ray study (right).

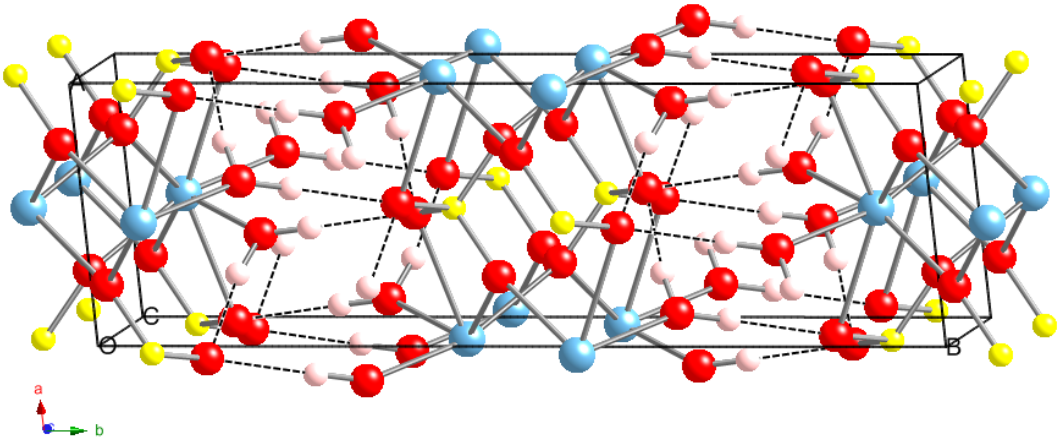

Figure 18 – the C2/c crystal structure of gypsum showing the layers linked by hydrogen bonding.

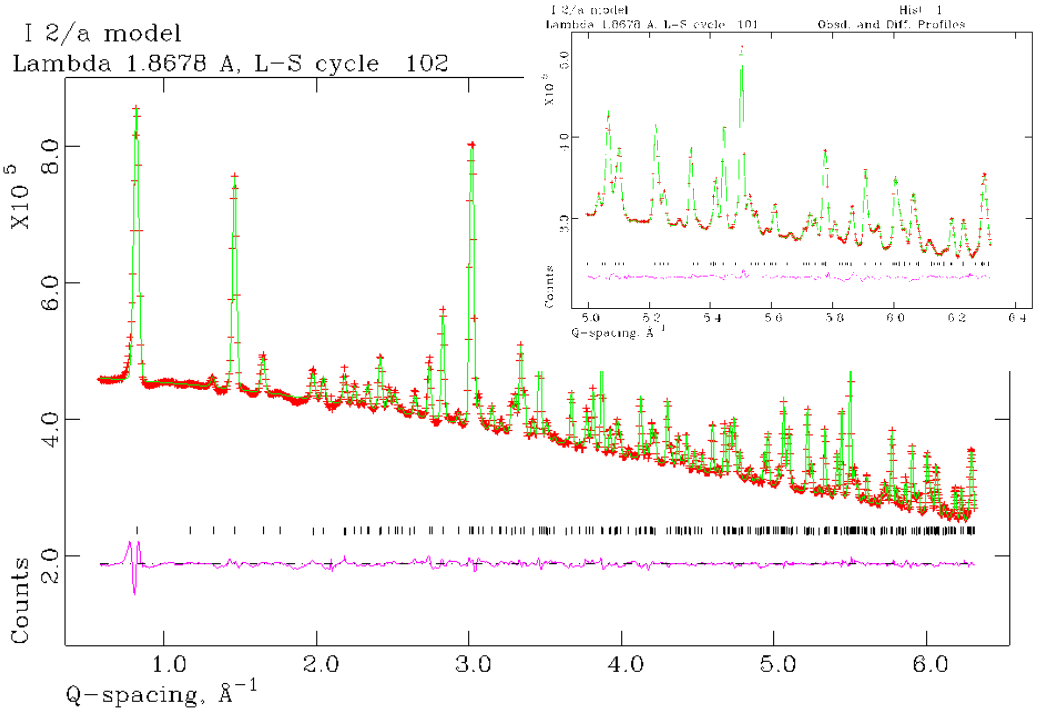

Figure 19 – final Rietveld refinement profile and fit for the D20 data from hydrogenous gypsum (1.87 Å incident wavelength). The inset shows the higher Q-space region.

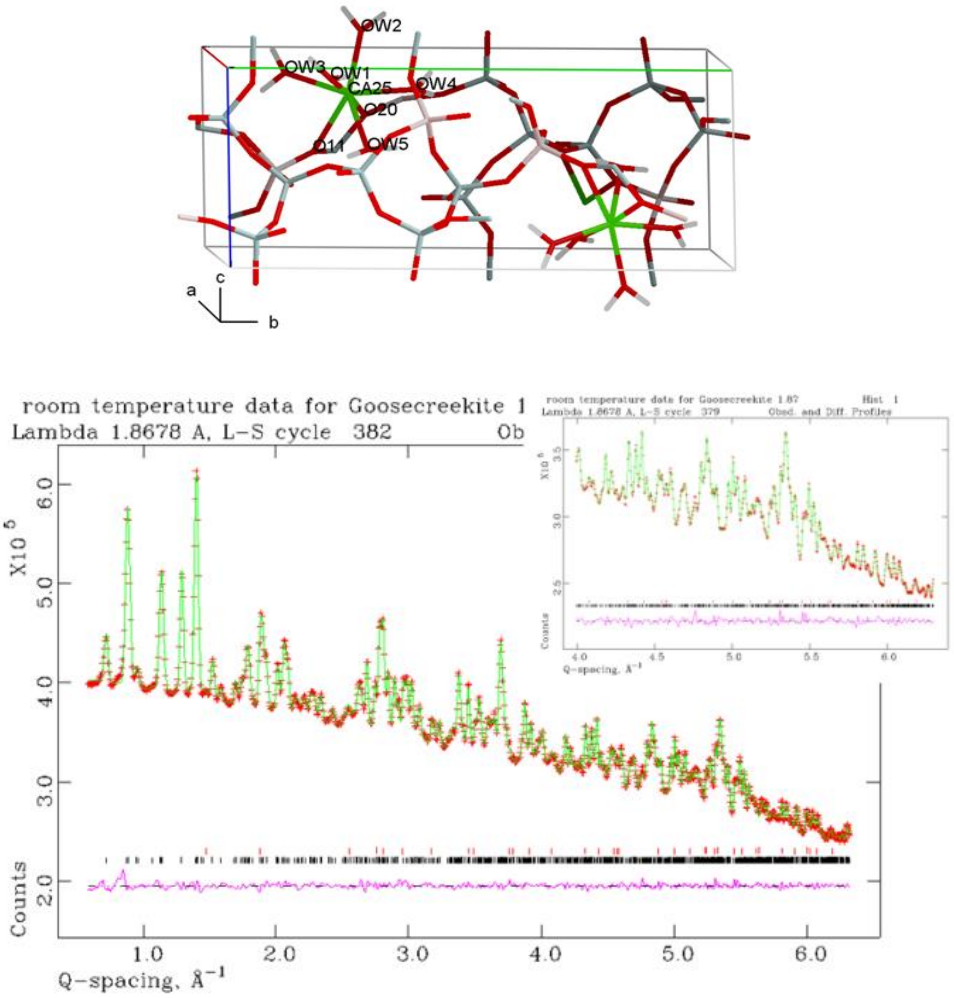

Figure 20 – the determined water structure in goosecreekite (top), and sample Rietveld fit to the NPD data (bottom).

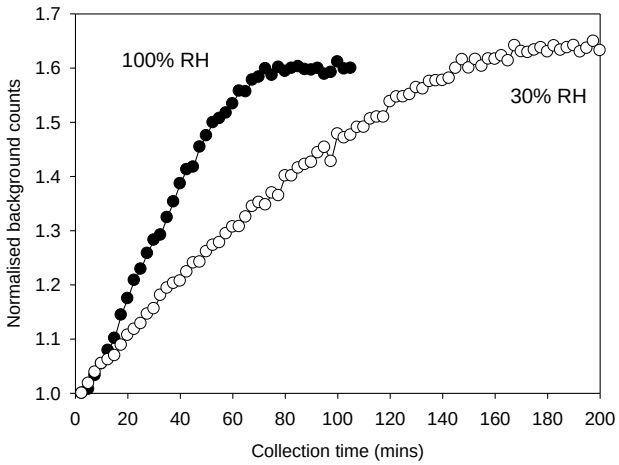

Figure 21 – Background count level of dried zeolite LTA samples exposed to 100% RH (black curve) and 30% RH (white curve) over time, as measured in-situ. Background counts were normalised to the background level at the start of the humidity ramp.

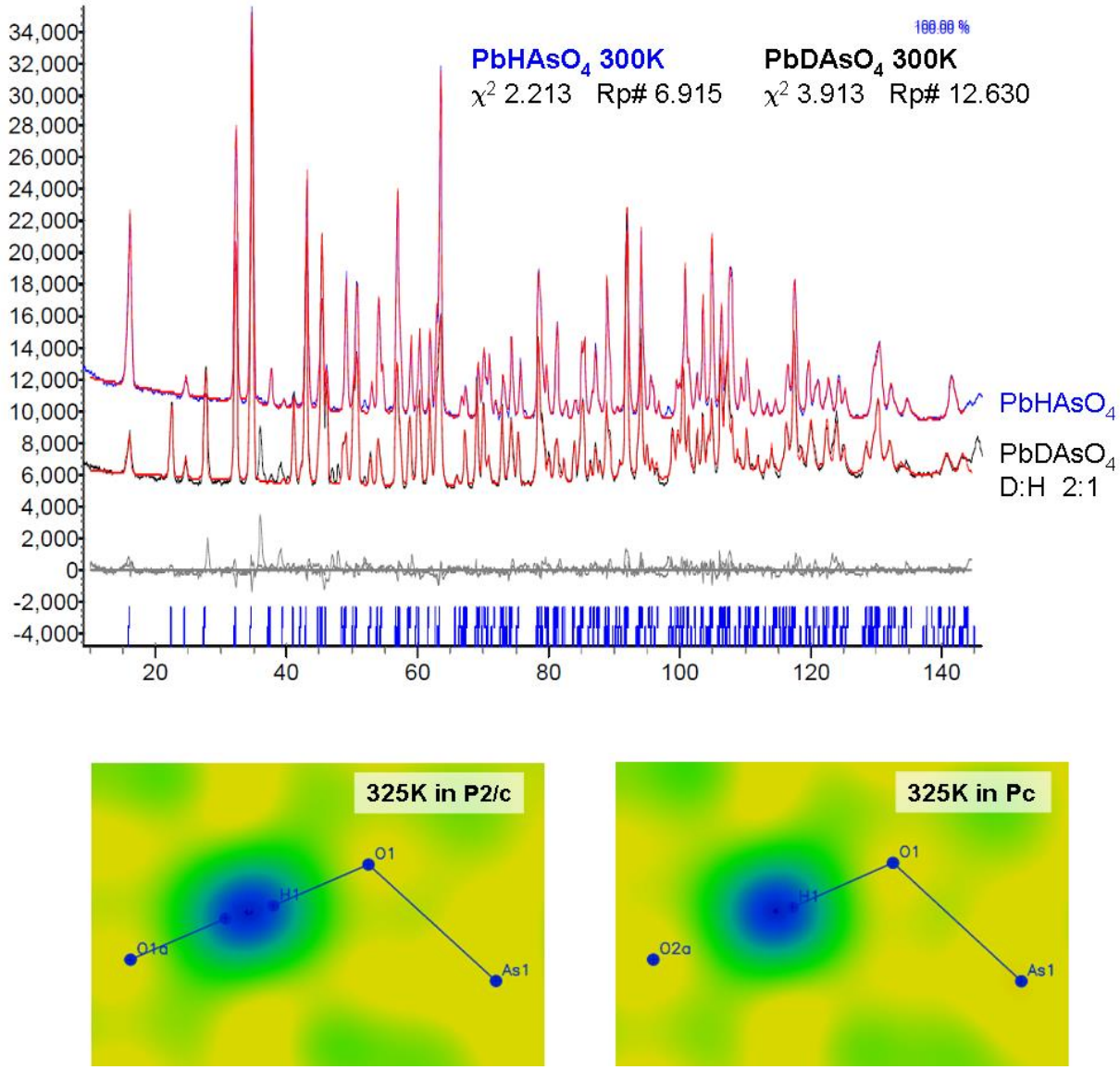

Figure 22 – NPD data and Rietveld fits for $PbHAsO_4$ and $PbDAsO_4$ (top), and Fourier difference maps calculated from the NPD data (bottom).

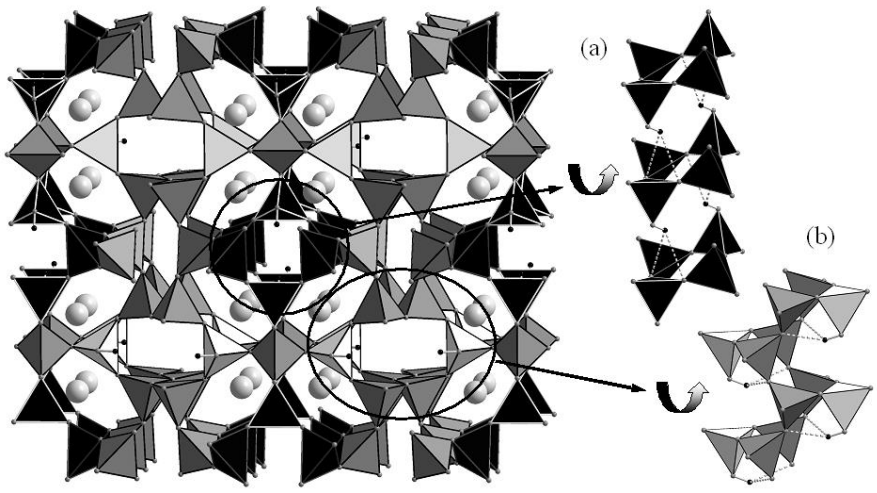

Figure 23 – overview (along b) and details of the structure of bavenite. (a) shows the environment of H2 with two weak hydrogen bonds to O3. (b) shows the environment of H1 forming two weak hydrogen bonds to O6. Be (T2) atoms within the very light gray tetrahedra, Si (T1, T5, T6) atoms within the medium gray tetrahedra, mixed Si/Al (T4) site within the dark gray tetrahedra, mixed Be/Al/Si (T3) site within the black tetrahedra with white borders, O atoms: small gray spheres, H atoms: small black spheres. H-bonds are drawn as dashed lines.

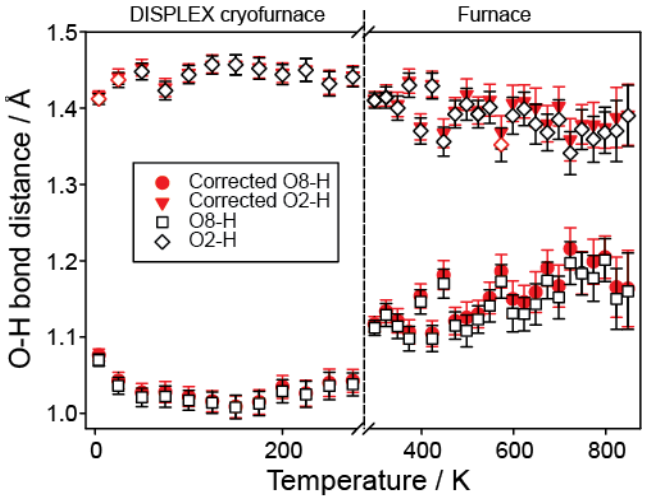

Figure 24 – the variation of the O(donor)-H and O(acceptor) H hydrogen bond lengths in ussingite as a function of temperature in the 4 ≤ T ≤ 850 K range.

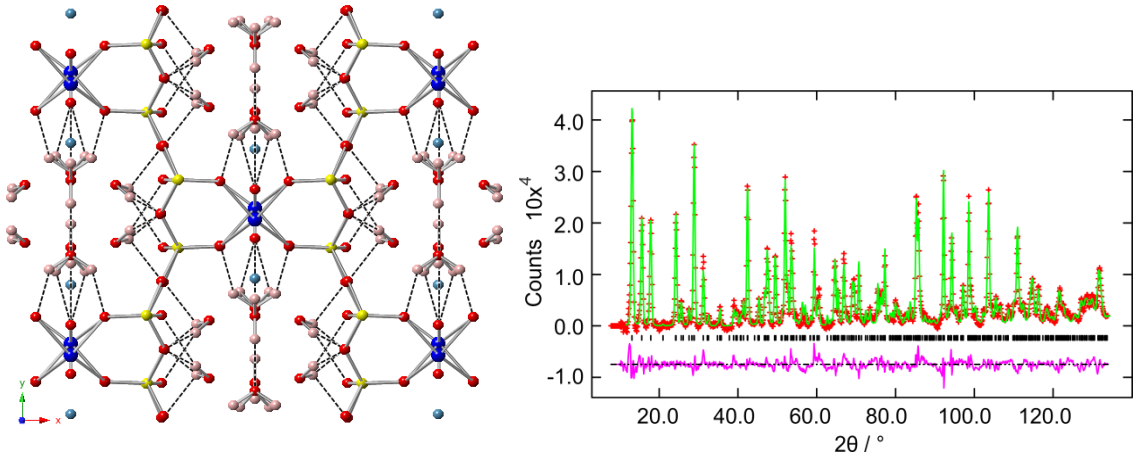

Figure 25 – (left) Crystal structure of pentagonite, showing the hydrogen bonding network within the pores; (right) Final Rietveld refinement profile fit for the D20 data for pentagonite at 120 K (λ=1.87 Å)

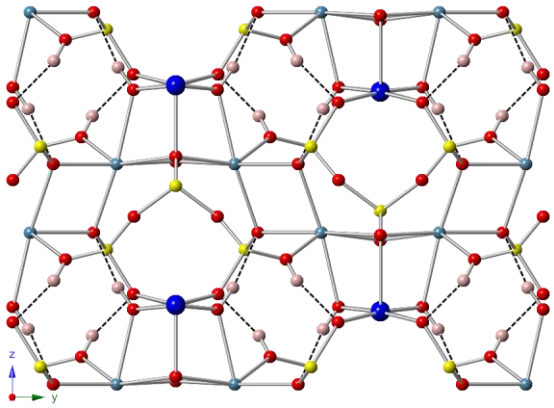

Figure 26 – crystal structure of kinoite, showing the inter- and intra-layer hydrogen bonding

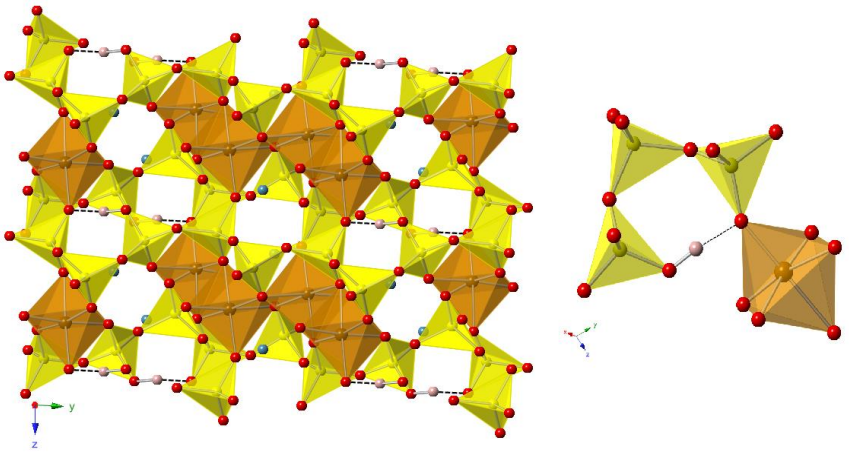

Figure 27 – crystal structure of babingtonite with, inset, the strong hydrogen bonding environment

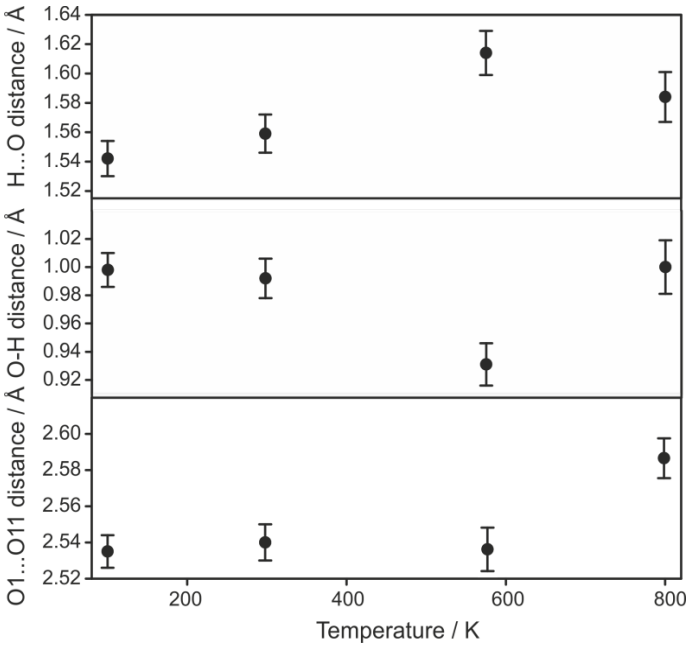

Figure 28 – variation in the O-H...O configuration in Babbingtonite as a function of temperature in the 100-800 K range.

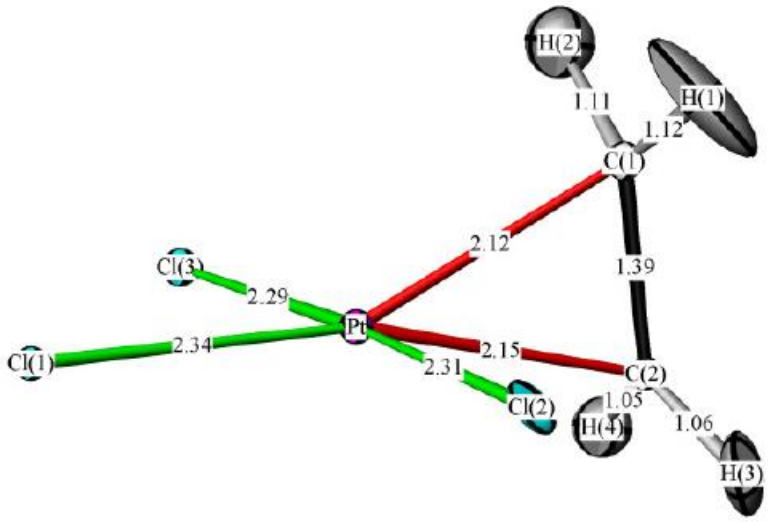

Figure 29 – Schematic view of the Structure of Zeise's salt refined from NPD data at 120 K, showing orientation of the C_2H_4 ligand and the anisotropic nature of the H atoms.

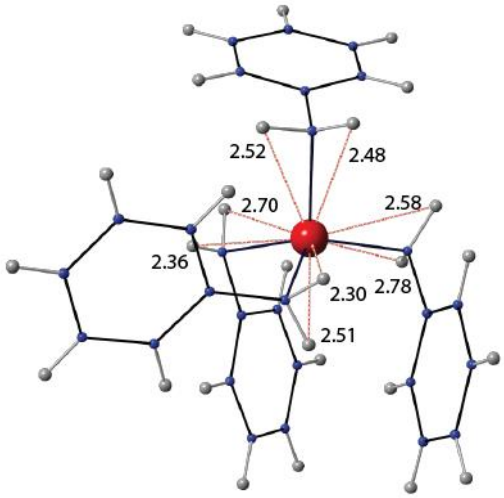

Figure 30 – the $Ti(CH_2C_6H_5)_4$ molecular unit showing the non-bonding (non-agostic) Ti…H distances. Ti-red, C-blue and H-grey.

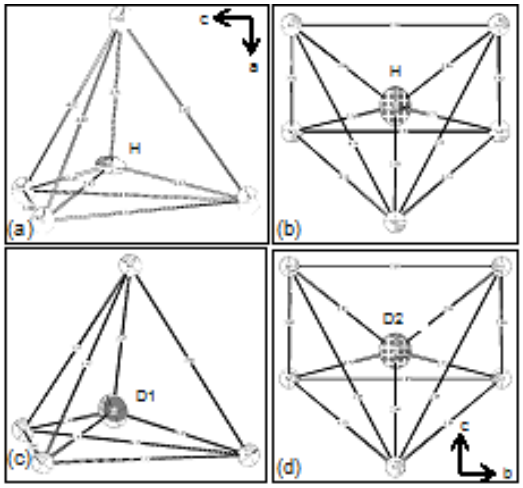

Figure 31 – the H/D environments in SrH_2/D_2: (a) H1; (b) H2; (c) D1 and (d) D2. The s.u. values from the NPD data for the refined Sr-Sr distances are in the range 0.00006 to 0.00011 Å and in the range 0.00004 to 0.00008 Å for the Sr-H/D distances.

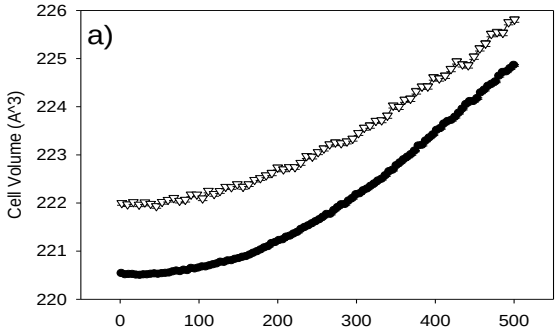

Figure 32 – The evolution of cell volume with temperature for SrH_2 (white triangles) and SrD_2 (black circles).

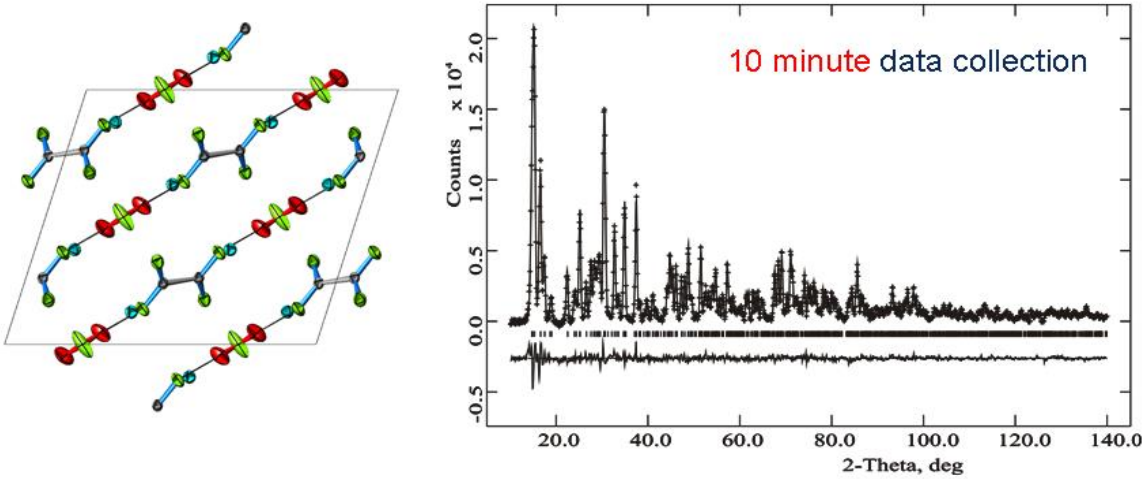

Figure 33 – structure of $Cs(C_2O_4).H_2O$ (left) determined from joint SCXD-NPD refinement, with the final NPD fit shown (right, from a 10 minute data collection

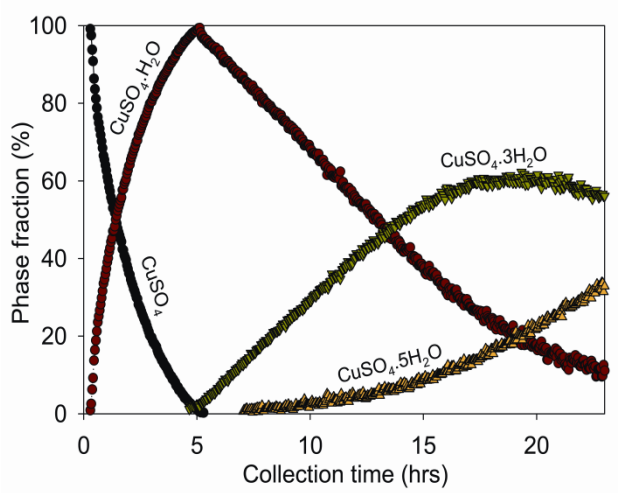

Figure 34 – the refined phase fractions of the anhydrous and hydrated phases of $CuSO_4$ as a function of exposure time at 100% RH, from the rapid scanning NPD data.